

Dependence of the transportation time on the sequence in which particles with different hopping probabilities enter a lattice

Hiroki Yamamoto^{1,*}, Daichi Yanagisawa^{2,3}, and Katsuhiro Nishinari^{2,3}

¹ *School of Medicine, Hirosaki University 5 Zaifu-cho Hirosaki city, Aomori Prefecture, 036-8562, Japan*

² *Research Center for Advanced Science and Technology, The University of Tokyo, 4-6-1 Komaba, Meguro-ku, Tokyo 153-8904, Japan*

³ *Department of Aeronautics and Astronautics, School of Engineering, The University of Tokyo, 7-3-1 Hongo, Bunkyo-ku, Tokyo 113-8656, Japan*

(Dated: April 11, 2019)

Smooth transportation has drawn the attention of many researchers and practitioners in several fields. In the present paper, we propose a modified model of a totally asymmetric simple exclusion process (TASEP), which includes multiple species of particles and takes into account the sequence in which the particles enter a lattice. We investigate the dependence of the transportation time on this ‘entering sequence’ and show that for a given collection of particles group sequence in some cases minimizes the transportation time better than a random sequence. We also introduce the ‘sorting cost’ necessary to transform a random sequence into a group sequence and show that when this is included a random sequence can become advantageous in some conditions. We obtain these results not only from numerical simulations but also by theoretical analyses that generalize the simulation results for some special cases.

I. INTRODUCTION

Transportation systems are key topics in social or biological systems [1]. In social systems, researchers have sought to obtain smooth transportation in various situations, such as production flow [2, 3], vehicular traffic [4–7], and pedestrian evacuation [8–11]. On the other hand, for biological systems, intracellular transportation along microtubules has been vigorously investigated [12–14].

Among various transportation models, the asymmetric simple exclusion process (ASEP), pioneered by MacDonald and Gibbs [15, 16], has attracted much attention. It is a stochastic process on a one-dimensional lattice in which particles move asymmetrically. A derivative of ASEP, in which particles are allowed to hop unidirectionally (left to right in the present paper) is called a totally asymmetric simple exclusion process (TASEP). In the field of nonequilibrium statistical mechanics, researchers have applied TASEP to various transportation problems, such as molecular-motor traffic [17–20], vehicular traffic [5–7, 21–23], and the exclusive-queuing process [24–26], especially since the latter has been solved exactly [27–29].

While many transportation problems consider the movements of a finite number of particles, TASEP studies usually investigate the steady state, without considering the number of particles. To investigate the problem of minimizing the transportation time for a finite number of particles, we propose here a modified TASEP. Our model differs from the original TASEP in four ways: we consider (i) a finite number of particles, (ii) multiple species of particles, (iii) the entering sequence of the particles, and (iv) the introduction of the sorting cost.

First, we take the number of particles to be finite and study the transportation times of those particles. Note

that we do not consider the steady state of the system itself. Minemura *et.al* [30] have investigated the transportation time for a hopping probability that depends upon the lot size, using the single-species TASEP with a finite number of particles. Other related works [31–34] have also adopted a finite number of particles. In those models, however, particles circulate through a system consisting of a lattice and a particle pool while the input or output rate is changed.

Second, multiple species of particles can exist, i.e., the hopping probabilities can differ among the particles. Almost all studies that have investigated smooth transportation have considered only one type of particle, even although in real-world situations there are various types of particles, e.g., pedestrians or vehicles, each moving at its own velocity. Although the concept of multiple hopping probabilities has itself already been studied extensively, most of these studies have focused on mathematically exact solutions to the systems and have not considered the application of the model to real-world situations. In addition, due to its simplicity, periodic-boundary conditions have been adopted in many studies [35–49]. Studies of multi-species ASEP with open boundaries have been started only recently [50–58]; for example, Ref. [58] obtained the exact phase diagram for a multi-species ASEP with open boundaries, although we note that they assumed multiple exchange rules, and not multiple hopping probabilities. In addition, those works adopted random updating. Our investigation focuses mainly on the problem of minimizing the transportation time, adopting open-boundary conditions and parallel updating. Note that—with the same boundary conditions and updating rules as the present paper—Ref. [59] adopted particles with disorder, whereas jumping particles were introduced in [60].

Third, we consider the entering sequence of particles. This is the most important feature of our model. To the

* h18m1140@hirosaki-u.ac.jp;

best of our knowledge, few TASEP investigations that focus on the entering sequence of the particles have been reported so far. In the present paper, we have considered two special types of sequences in particular: ‘random sequences’ and ‘group sequences,’ and we have compared the transportation times for these two types of sequences.

Finally, we introduce the sorting cost in our model. With no sorting, particles are usually transported at random, i.e., in a random sequence. It is therefore useful to consider the cost of sorting particles from a random sequence into a group sequence. In the present paper, we define this sorting cost and compare the results with and without sorting.

We have determined the dependence of the transportation time on the entering sequence of the particles from numerical simulations based on our model. Moreover, we find that the optimal sequence can vary, depending upon choice of parameter set, when the sorting cost is considered. In addition, we have succeeded in obtaining mathematical proofs of the simulation results for some special cases.

In real situations, our proposed method can be interpreted as smooth logistics for various types of products or as an effective method of evacuation from sports stadiums, concert venues, and so on.

The remainder of the present paper is organized as follows. Section II describes the details of our proposed model and some important parameters, modifying the original TASEP. In Sec. III, we present and discuss the results of numerical simulations using the modified TASEP. Section IV presents theoretical analyses of the simulation results for some special cases. The paper concludes in Sec. V.

II. MODEL DESCRIPTION

A. Original (single-species) TASEP with open-boundary conditions

The original TASEP with open-boundary conditions is defined as a one-dimensional lattice of L sites, labeled from left to right $i = 0, 1, \dots, L - 1$ (see Fig. 1). Each site can be either empty or occupied by a single particle. In the present paper, we adopt discrete time steps and parallel updating. In parallel updating, the states of all the particles on the lattice are determined simultaneously in the next time step. Particles enter the lattice from the left boundary with probability α , and leave the lattice from the right boundary with probability β . In the bulk of the lattice, if the right-neighboring site is empty, a particle hops to that site with probability p ; otherwise it remains at its present site. Our modified TASEP differs from this original one in the following four ways.

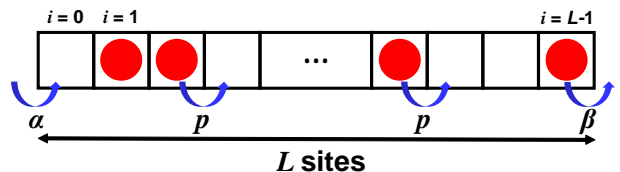


FIG. 1. (Color online) Schematic illustration of the original TASEP with open-boundary conditions.

B. Difference 1: Finite number of particles

First, the number of particles N is finite, as illustrated in Fig. 2. The system evolves until the N th particle leaves the lattice. We define the transportation time T as the time gap between the start of the simulation and the time when the N th particle leaves the lattice.

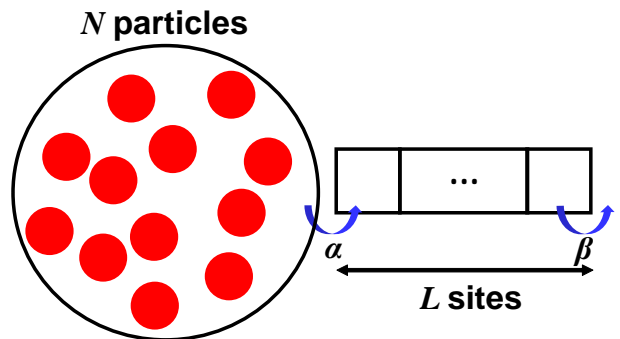


FIG. 2. (Color online) Schematic illustration of TASEP with a finite number of particles. This figure shows the case $N = 12$.

C. Difference 2: Multi-species particles

Second, our model adopts multi-species particles, i.e., particles with different hopping probabilities, as illustrated in Fig. 3. Specifically, each of the N particles is allocated to one of S species, where $1 \leq S \leq N$. Particles that belong to each species s ($s = 1, 2, \dots, S$) all have the same hopping probability $p = p_s$ ($0 < p_s \leq 1$). Note that with $S = 1$ our model reduces to the single-species TASEP, whereas with $S = N$ all particles have different hopping probabilities. The fraction of all the N particles allocated to each species s is defined as r_s , obviously satisfying $\sum_{s=1}^S r_s = 1$.

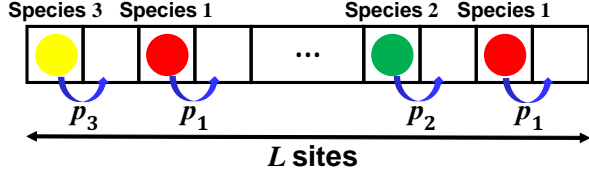


FIG. 3. (Color online) Schematic illustration of TASEP with multi-species particles. In this figure, we show a case with $S = 3$, where the red particles belong to species 1, green ones to species 2, and the yellow ones to species 3.

D. Difference 3: Consideration of entering sequence of particles

Third, we consider the sequence in which the particles enter the lattice (i.e., the ‘entering sequence’), which is the most important feature in our model. Specifically, particles form a queue before the left boundary and enter the lattice according to the sequence, as illustrated in Fig. 4. In the present paper, we investigate two types of sequences: ‘random sequences’ and ‘group sequences,’ as illustrated in Fig. 5.

In a random sequence, particles line up randomly regardless of their hopping probabilities. A random sequence thus has $N! / \prod_{s=1}^S (r_s N)!$ patterns. Note that in real situations without any controls, random sequences can be assumed to occur spontaneously.

On the other hand, in a group sequence, particles form groups of the same species and line up group by group. There are $S!$ possible patterns of group sequences, which are clearly among the random sequences.

For the case $S = N$, where all hopping probabilities are different, we bunch the particles with similar hopping probabilities close together with each other as much as possible, imaginarily considering them as ‘continuous groups.’ Consistent with this idea, we define a group sequence with $S = N$ as either an ascending or a descending sequence. Note that we define such a sequence by considering the rightmost particle to be the first particle in the sequence.

We define the transportation times for the random and group sequences to be T_R and T_G , respectively.

E. Difference 4: Introduction of the sorting cost

Finally, we introduce the cost of sorting the particles and investigate the effect of the sorting cost on the transportation time. Here, we define the sorting cost as the minimal number of exchanges $K(\tau_a, \tau_b)$ necessary to sort the particles from sequence τ_b to sequence τ_a , where τ_a and τ_b represent the sequence after sorting and before sorting, respectively. Note that the arguments of $K(\tau_a, \tau_b)$ will be abbreviated in obvious cases.

In the present paper, τ_a (τ_b) correspond to τ_G (τ_R),

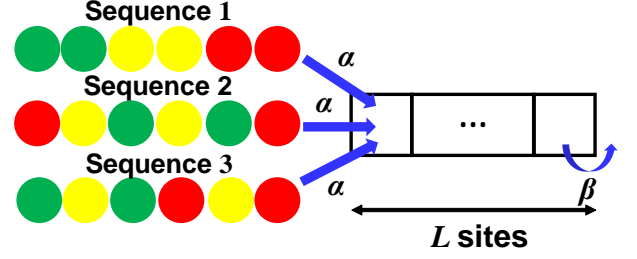


FIG. 4. (Color online) Schematic illustration of the entering sequences of particles. In this figure, we show three examples among all $90 \{= 6! / (2!2!2!)\}$ possible sequences for the case $N = 6$, $S = 3$, and $r_1 = r_2 = r_3 = 1/3$. Note that Sequence 1 is one example of a group sequence, whereas the others are examples of random sequences.

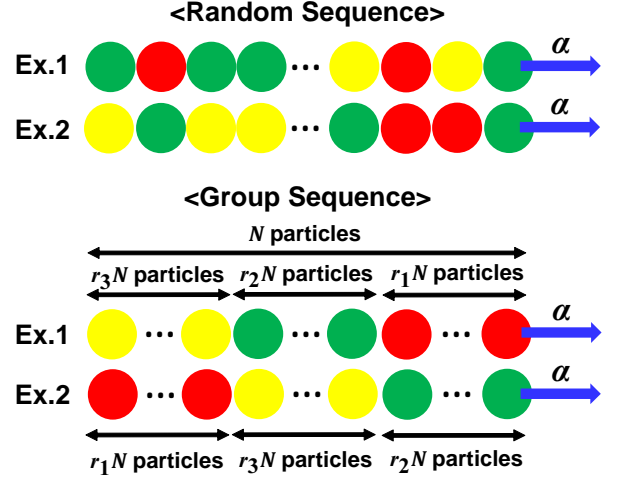


FIG. 5. (Color online) Schematic illustration of random (upper panel) and group (lower panel) sequences for $S = 3$, where the red particles belong to species 1, the green ones to species 2, and the yellow ones to species 3. In the upper panel, we show two possible examples out of all $N!$ possible random sequences, whereas in the lower panel, we display two examples of all $6 (= 3!)$ possible group sequences. Note that in each case $r_1 + r_2 + r_3 = 1$.

where τ_R and τ_G represent a random sequence and a group sequence, respectively. The sequence τ_G can differ depending upon τ_R ; that is, τ_G is determined so that the number of exchanges is minimized for each τ_R . Figure 6 shows two examples for which $K(\tau_a, \tau_b) = 2$ when $N = 6$ and $S = 3$. Note that we do not consider the distance between the exchanged particles.

We define the number of time steps necessary to sort the particles to be λK , where the parameter λ is the ratio of the sorting cost to number of TASEP time steps.

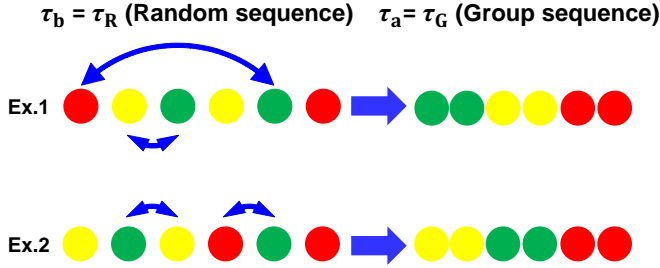


FIG. 6. (Color online) Two examples with $K(\tau_a, \tau_b) = 2$ for the case $N = 6$ and $S = 3$. For each sequence τ_R , we chose the one of all $6 (= 3!)$ possible sequences τ_G so that $K(\tau_a, \tau_b)$ is minimized.

III. SIMULATION RESULTS

In this section, we use numerical simulations to investigate the dependence of the transportation time on the entering sequence of the particles.

In all the simulations below, we set $L = 200$ and $N = 10,000$; we validate this selection of L and N in Appendix A. We determine the value of T for each parameter, and average T over 100 trials for Fig. 7 and over 10 trials for Figs. 8, 9, and 10).

A. Without sorting cost ($\lambda = 0$)

In this subsection, we set $\lambda = 0$, i.e., we do not include the sorting cost.

In Fig. 7 we plot the simulation values of the number of particles that have not yet exited the lattice at time t for $S \in \{2, 3, N\}$. We fix $(\alpha, \beta) = (1, 1)$ for (a)–(c) and $(\alpha, \beta) = (0.1, 0.2)$ for (d)–(f). In the figures, we refer to the number of particles that have not yet exited the lattice at time t simply as the ‘remaining particles.’ The simulation starts at $t = 0$, and the number of particles becomes 0, i.e., the N th particle exits the lattice, at $t = T$.

We note two important phenomena in Figs. 7 (a)–(c). First, surprisingly, T_G is smaller than T_R for all three values of S when $\alpha = \beta = 1$. This result implies that the group sequences yield smoother transportation than the random ones for the cases $(\alpha, \beta) = (1, 1)$. Second, T_G seems not to depend upon the order of each group in the group sequence, which can take $S!$ possible patterns.

On the other hand, in Figs. 7 (d)–(f), unlike the cases in Figs. 7 (a)–(c), the difference between T_R and T_G seems to vanish.

In order to compare the difference between T_R and T_G for various (α, β) , we define Δ_T as the ratio of the change from T_R to T_G ; that is,

$$\Delta_T = \frac{T_G - T_R}{T_R}. \quad (1)$$

From this definition of Δ_T , $\Delta_T < 0$ ($\Delta_T > 0$) indicates that group (random) sequences are preferable for smooth transportation. Note that in the following, to calculate Δ_T we assume that each group in a group sequence is arranged in ascending order in terms of species number s .

The simulation values of Δ_T for various (α, β) with (a) $S = 2$, (b) $S = 3$, and (c) $S = N$ are plotted in Fig. 8. Note that the black lines represent the boundaries between the low-density/high-density (LD/HD) and the maximal current (MC) phases of the single-species TASEP with hopping probability p_1 (boundary A) in Fig. 8 (a), and p_1 (boundary B1) and p_3 (boundary B3) in Fig. 8 (b), respectively.

Figure 8 shows that for all three values of S , Δ_T is small in the region where $\min(\alpha, \beta)$ is relatively large. [In Fig. 8 (b), Δ_T finally yields to a constant value in the upper-right region beyond boundary B3.] On the other hand, Δ_T is small in the region where $\min(\alpha, \beta)$ is relatively small. [In Fig. 8 (a) and (b), Δ_T is almost 0, especially in the lower-left region beyond the boundary A or B1.] Here, we term the region with $\Delta_T < 0$ as the ‘group-advantageous region’ ($T_R > T_G$), whereas we designate the region with $\Delta_T \approx 0$ as a ‘neutral region’ ($T_R \approx T_G$), if it exists.

These results indicate that group sequences can make transportation smoother than random sequences when the system is mainly governed by the bulk region of the lattice, but the dependence on the type of sequences vanishes (or decreases) when the system is mainly governed by the boundaries.

B. With sorting cost ($\lambda > 0$)

In this subsection, we consider the sorting cost by varying λ for the same parameter sets in the previous subsection. Appendix B presents specific schemes for obtaining the minimal number of exchanges necessary to sort the particles in the simulations.

Figure 9 plots Δ_T for (a) $S = 2$, (b) $S = 3$, and (c) $S = N$ as functions of λ for various $(\alpha, \beta) \in \{(0.1, 0.2), (0.6, 0.6), (1, 1)\}$, which are plotted as black crosses in Fig. 8. We emphasize again that in the region with $\Delta_T < 0$ group sequences are preferred, even if when the sorting cost is considered, whereas in the region with $\Delta_T > 0$ random sequences are preferred. Note that the cases with $\lambda = 0$ correspond to those obtained without considering the sorting cost.

As discussed in the previous subsection, we note that $\Delta_T \leq 0$ for almost all (α, β) when $\lambda = 0$, indicating that sorting is almost always beneficial for smooth transportation. However, once the sorting cost is considered, the sign of Δ_T can become positive, especially in the region where $\min(\alpha, \beta)$ is relatively small, indicating that sorting is not always beneficial. Note that the curves of $(\alpha, \beta) = (0.6, 0.6)$ and $(1, 1)$ are observed to overlap each other in Fig. 9 (b) and (c), unlike Fig. 9 (a). This hap-

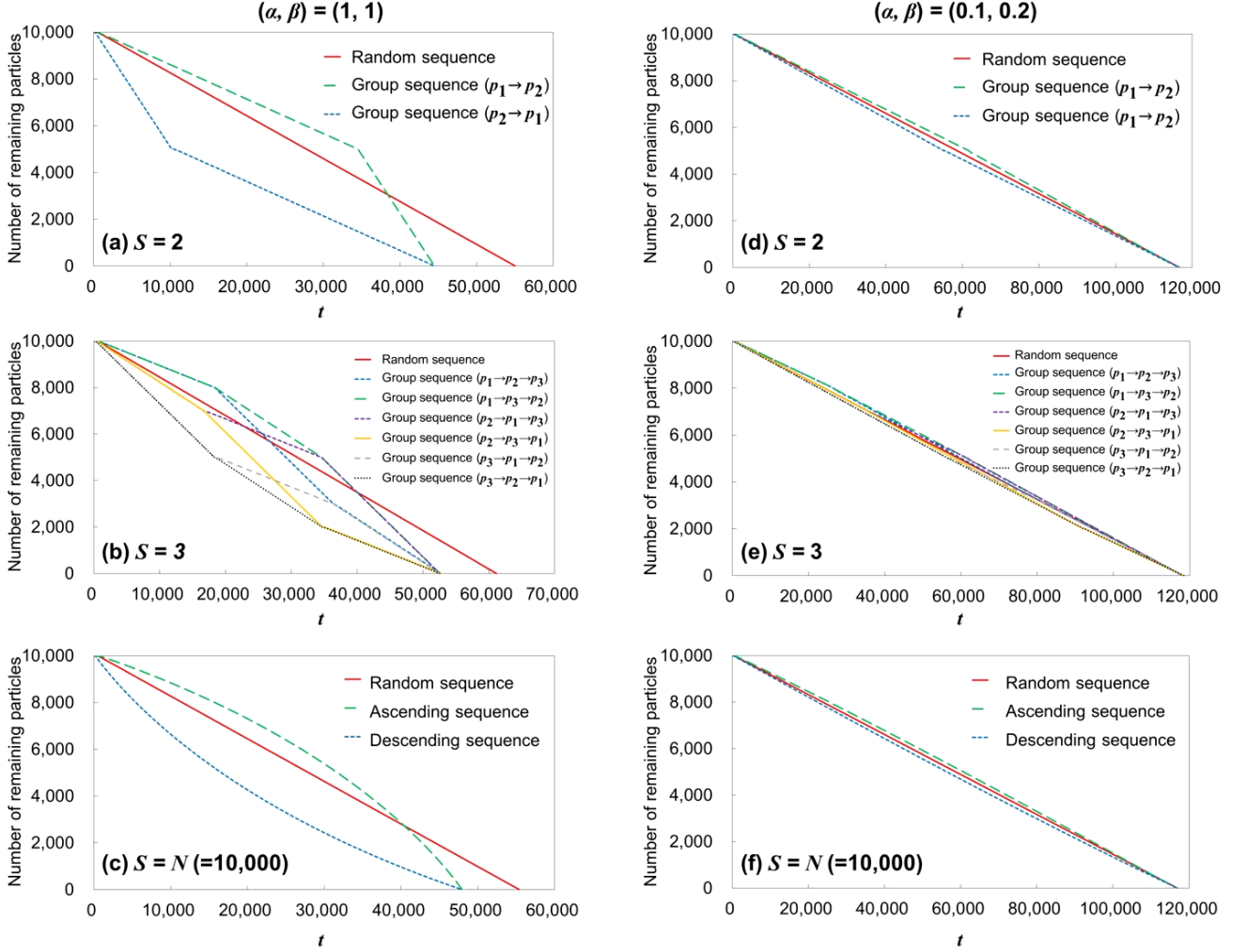


FIG. 7. (Color online) Simulation values of the number of particles remaining at time t with $\lambda = 0$ for (a) $S = 2$, (b) $S = 3$, and (c) $S = N$ with $(\alpha, \beta) = (1, 1)$, and for (d) $S = 2$, (e) $S = 3$, and (f) $S = N$ with $(\alpha, \beta) = (0.1, 0.2)$. For $S = 2$, $S = 3$, and $S = N$, respectively, we set $(p_1, p_2; r) = (0.5, 1; 0.5)$, $(p_1, p_2, p_3; r_1, r_2, r_3) = (0.4, 0.6, 0.8; 0.2, 0.3, 0.5)$, and $p_s = 1 - 0.6(N - s)/(N - 1)$ ($s = 1, 2, \dots, N$), respectively, fixing $\lambda = 0$. The notation ' $p_s \rightarrow p_t$ ' means that a group of species s is followed by a group of species t .

pens because there is no difference in Δ_T at these two points when $\lambda = 0$, as we can see in Figs. 8 (b) and (c).

Figure 10 plots Δ_T for (a) $S = 2$, (b) $S = 3$, and (c) $S = N$ for various (α, β) with $\lambda = 1$. In this figure, we note the existence of a new region in which $\Delta_T > 0$, which we term a 'random-advantageous region' ($T_R < T_G$). This new region widens as λ increases, finally resulting in the complete disappearance of the group-advantageous region for large enough λ . Note that Fig. 10 (c) exhibits only a random-advantageous region.

IV. THEORETICAL ANALYSES

In this section, we show that the simulation results can be theoretically reproduced in some special cases. Specifically, we have succeeded in obtaining a mathemat-

ical proof of the appearance of the group-advantageous region for any group number $S (> 1)$ when $\lambda = 0$.

A. Approximate flow of a multi-species TASEP

In this subsection, before calculating T , we briefly discuss the steady-state flow Q_S of the multi-species TASEP that corresponds to a random sequence. We write $Q_S = Q_S(p_1, \dots, p_S; r_1, \dots, r_S)$, with the arguments abbreviated in obvious cases. When the flow Q is simulated for each parameter set, we first evolve the system for 10^5 time steps and then average over the next 10^6 time steps.

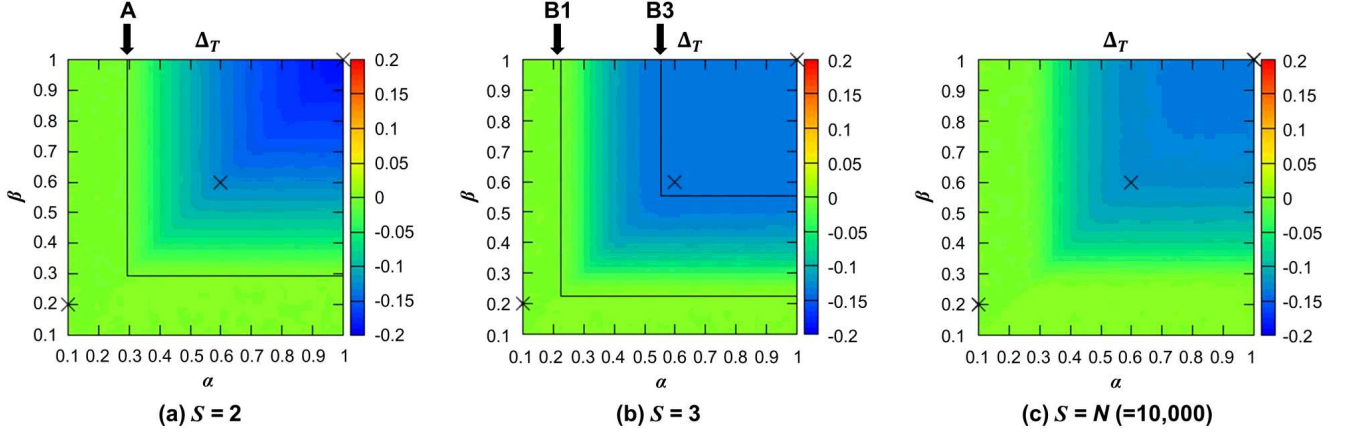


FIG. 8. (Color online) Simulation values of Δ_T for various (α, β) with (a) $S = 2$, (b) $S = 3$, and (c) $S = N$. The parameters other than (α, β) are the same as in Fig. 7. Note that three black crosses in each panel represent $(\alpha, \beta) = (0.1, 0.2)$, $(0.6, 0.6)$, and $(1, 1)$, respectively. The color scale at the right of each panel represents the value of Δ_T .

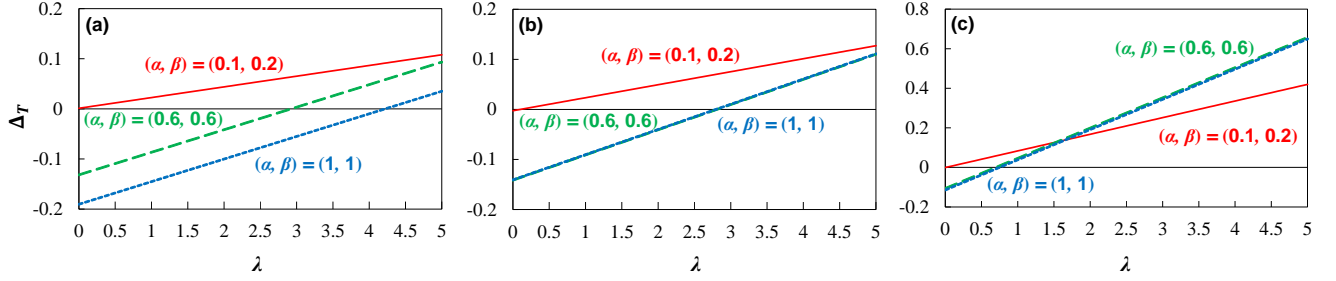


FIG. 9. (Color online) Simulation values of Δ_T with (a) $S = 2$, (b) $S = 3$, and (c) $S = N$ as functions of λ for various $(\alpha, \beta) \in \{(0.1, 0.2), (0.6, 0.6), (1, 1)\}$. The parameters other than (α, β) are the same as in Fig. 7.

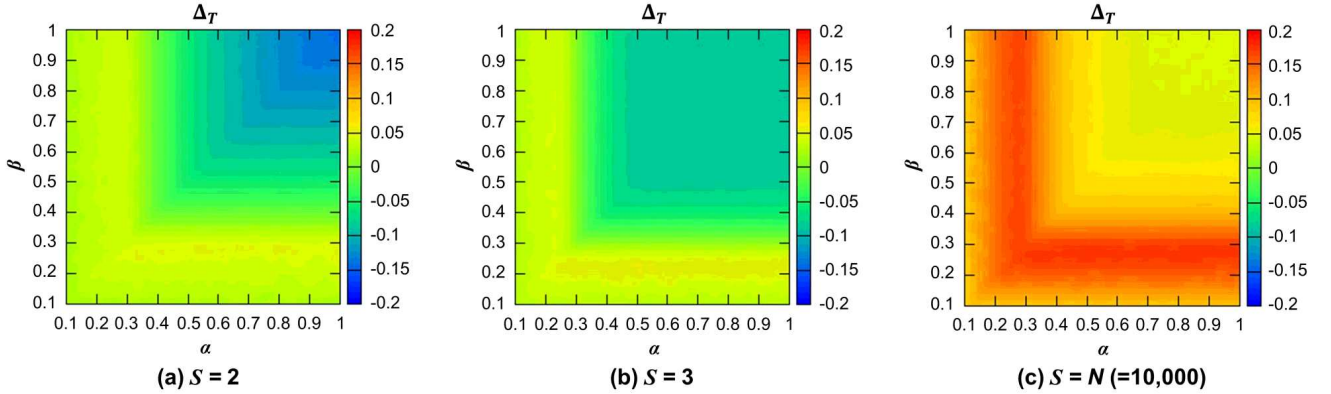


FIG. 10. (Color online) Simulation values of Δ_T for various (α, β) with (a) $S = 2$, (b) $S = 3$, and (c) $S = N$ for $\lambda = 1$. The other parameters are the same as in Fig. 7.

$$\begin{pmatrix} P_{00} \\ P_{01} \\ P_{02} \\ P_{10} \\ P_{11} \\ P_{12} \\ P_{20} \\ P_{21} \\ P_{22} \end{pmatrix} = \begin{pmatrix} 1-\alpha & (1-\alpha)\beta & (1-\alpha)\beta & 0 & 0 & 0 & 0 & 0 & 0 \\ 0 & (1-\alpha)(1-\beta) & 0 & p_1 & 0 & 0 & 0 & 0 & 0 \\ 0 & 0 & (1-\alpha)(1-\beta) & 0 & 0 & 0 & p_2 & 0 & 0 \\ r\alpha & r\alpha\beta & r\alpha\beta & 1-p_1 & \beta & \beta & 0 & 0 & 0 \\ 0 & r\alpha(1-\beta) & 0 & 0 & 1-\beta & 0 & 0 & 0 & 0 \\ 0 & 0 & r\alpha(1-\beta) & 0 & 0 & 1-\beta & 0 & 0 & 0 \\ (1-r)\alpha & (1-r)\alpha\beta & (1-r)\alpha\beta & 0 & 0 & 0 & 1-p_2 & \beta & \beta \\ 0 & (1-r)\alpha(1-\beta) & 0 & 0 & 0 & 0 & 0 & 1-\beta & 0 \\ 0 & 0 & (1-r)\alpha(1-\beta) & 0 & 0 & 0 & 0 & 0 & 1-\beta \end{pmatrix} \begin{pmatrix} P_{00} \\ P_{01} \\ P_{02} \\ P_{10} \\ P_{11} \\ P_{12} \\ P_{20} \\ P_{21} \\ P_{22} \end{pmatrix} \quad (2)$$

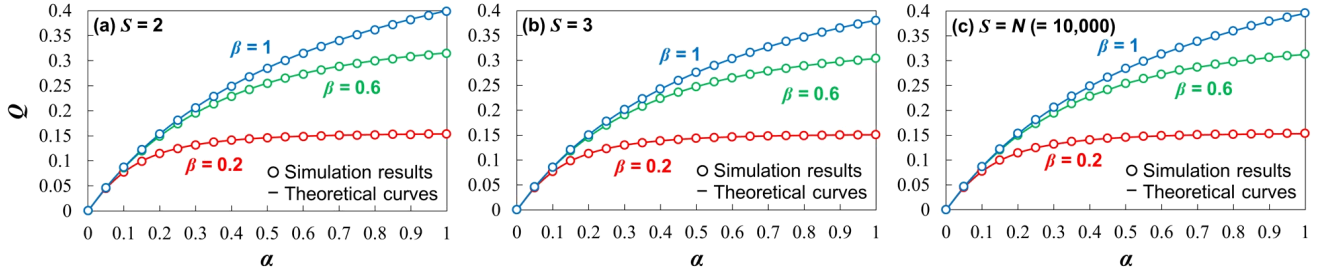


FIG. 11. (Color online) Simulation (circles) and theoretical (curves) values of (a) Q_2 , (b) Q_3 , and (c) Q_S for $L = 2$ as functions of α for various $\beta \in \{0.2, 0.6, 1\}$. The other parameters are fixed at (a) $(p_1, p_2; r) = (0.5, 1; 0.5)$, (b) $(p_1, p_2, p_3; r_1, r_2, r_3) = (0.4, 0.6, 0.8; 0.2, 0.3, 0.5)$, (c) $p_s = 1 - 0.6(S - s)/(S - 1)$ ($s = 1, 2, \dots, N$) and $r_s = 1/N (= 1/10,000)$.

1. $L = 2$

This subsection presents the derivation of an approximate Q_S based on a Markov chain model. Due to the difficulty of considering general values of L (the length of the lattice) and S (the number of particle species), we consider the simplest case—with $L = 2$ and $S = 2$. As two species of particles exist—that is, particles with hopping probability p_1 and particles with p_2 —each site may have three states: ‘unoccupied (state 0),’ ‘occupied by a particle 1 (state 1),’ and ‘occupied by a particle 2 (state 2).’ This results in $9 (= 3 \times 3)$ possible states. Here, we define the probability distribution P_{ij} ($i, j = 0, 1, 2$), where i and j represent the state number of site 1 and 2, respectively. The master equations for the steady state are summarized in Eq. (2), using the relation $r_1 (= r) + r_2 = 1$. Note that r_1 and r_2 are replaced with r and $1 - r$, respectively, for the case $S = 2$.

In addition, P_{ij} must satisfy the normalization condition

$$\sum_{i=0}^2 \sum_{j=0}^2 P_{ij} = 1. \quad (3)$$

From Eqs. (2) and (3), the flow of the system can be written as a function of p_1 , p_2 , and r ; that is, $Q_2(p_1, p_2; r)$, is given by the following expression:

$$\begin{aligned} Q_2(p_1, p_2; r) &= p_1 P_{10} + p_2 P_{20} \\ &= \frac{p_1 p_2 A}{p_1 p_2 B + \{(1 - r)p_1 + r p_2\} A}, \end{aligned} \quad (4)$$

where

$$A = \alpha\beta(\alpha + \beta - \alpha\beta) \quad (5)$$

and

$$B = \alpha^2 + \beta^2 - \alpha^2\beta - \alpha\beta^2 + \alpha\beta. \quad (6)$$

For $r = 1$ and $p_1 = p$, the system reduces to the single-species TASEP with the flow $Q_1(p)$, where

$$Q_1(p) = \frac{pA}{pB + A}. \quad (7)$$

Therefore, assuming that the value $p = p_h$ satisfies the condition $Q_2(p_1, p_2; r) = Q_1(p)$, we can derive

$$p_h = \frac{p_1 p_2}{(1 - r)p_1 + r p_2}. \quad (8)$$

The quantity p_h is termed the harmonic mean of p_1 and p_2 . Accordingly, for $L = 2$, Q_2 is equivalent to $Q_1(p = p_h)$. This relation holds for any species number $S(> 2)$, as we show by mathematical induction in Appendix C.

Figure 11 compares the simulation and theoretical curves for various $\beta \in \{0.2, 0.6, 1\}$ with (a) $S = 2$, (b) $S = 3$ and (c) $S = N (= 10,000)$. In all the figures, the simulations show very good agreement with our exact analyses.

2. General $L(> 2)$

For general $L(> 2)$ and $S(> 1)$, it is complicated to solve the master equations. Therefore, in this subsection, we instead introduce an inequality, based on the discussions in the previous subsection.

First, for general L and S , Q_S is clearly larger than $Q_1(p = p_{\min})$, where $p_{\min} = \min\{p_1, p_2, \dots, p_S\}$.

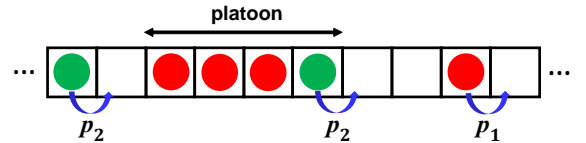


FIG. 12. (Color online) Schematic illustration of a platoon. In this figure, we set $S = 2$, with the red particles belonging to species 1 (faster) and the green ones to species 2 (slower). A green particle blocks the red particles behind it, so that the trailing red particles cannot hop with probability p_1 but only with probability p_2 , which is less than p_h .

In addition, for $L > 2$, a platoon can be observed in the bulk of the lattice, in which a slower particle behaves as a bottleneck, and faster particles behind it cannot hop with a probability larger than that of the smaller one,

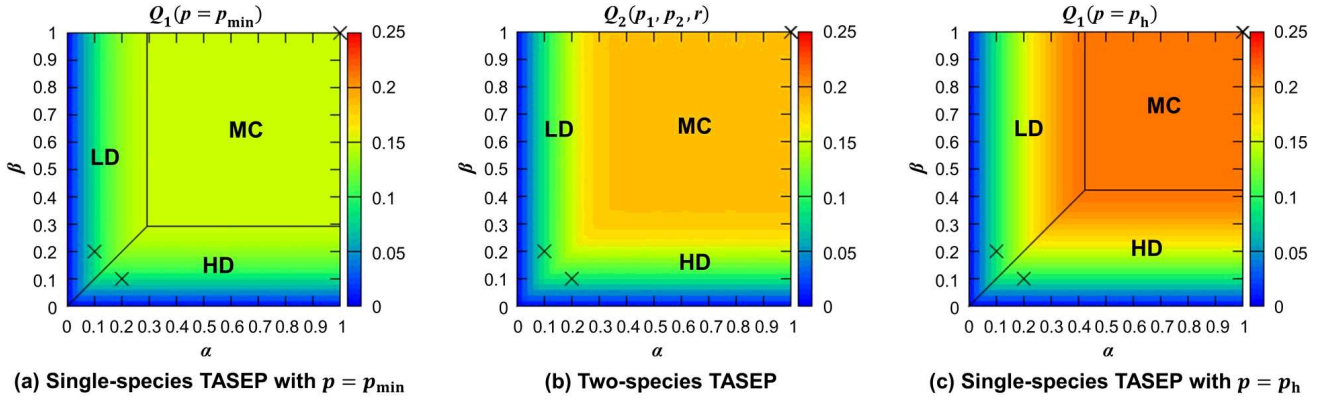


FIG. 13. (Color online) Phase diagrams. The color bars indicate the simulation values of (a) $Q_1(p = p_{\min})$, (b) $Q_2(p_1, p_2; r)$, and (c) $Q_1(p = p_h)$, respectively, obtained by fixing $(p_1, p_2; r) = (0.5, 1; 0.5)$, $p_{\min} = 0.5$, and $p_h = 1/(0.5/0.5 + 0.5/1) = 2/3$. Note that the three black crosses in each figure represent $(\alpha, \beta) = (0.1, 0.2)$, $(0.2, 0.1)$, and $(1, 1)$, respectively.

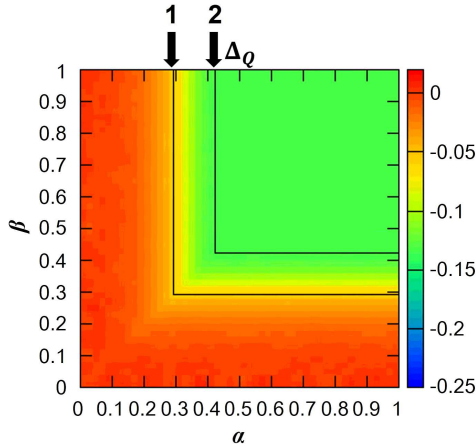


FIG. 14. (Color online) Calculated values of Δ_Q for various (α, β) , fixing $(p_1, p_2; r) = (0.5, 1; 0.5)$.

i.e., less than p_h , as shown in Fig. 12. This phenomenon suppresses the flow, implying that Q_S is smaller than $Q_1(p = p_h)$.

Consequently, Q_S satisfies the following inequality;

$$Q_1(p = p_{\min}) < Q_S < Q_1(p = p_h). \quad (9)$$

In this subsection, we hereafter consider the case $S = 2$.

Figure 13 shows the phase diagrams obtained by plotting the simulation values for (a) the single-species TASEP with $p = p_{\min}$, (b) the two-species TASEP, and (c) the single-species TASEP with $p = p_h$, respectively. Note that Q_2 (Q_1) are the simulation (theoretical) values (and similarly hereafter).

Comparing these three figures shows that Eq. (9) obviously holds. In addition, as in Figs. 13 (a) and (c), we find that three different phases—HD, LD, and MC—also exist in Fig. 13 (b). Due to Eq. (9), the boundaries between the LD (HD) and MC phases of Fig. 13 (b) lie

between those of Figs. 13 (a) and 13 (c). Note that the black lines in Figs. 13 (a) and (c) are theoretical boundaries, based on the fact that the boundary between the LD and MC phases of the single-species TASEP with hopping probability p [27] can be written as

$$\begin{cases} \alpha = 1 - \sqrt{1-p} \wedge 1 - \sqrt{1-p} < \beta < 1 \\ \beta = 1 - \sqrt{1-p} \wedge 1 - \sqrt{1-p} < \alpha < 1 \end{cases} \quad (10)$$

Here, as for Δ_T , we define Δ_Q as the ratio of the change from $Q_1(p = p_h)$ to Q_2 ; that is,

$$\Delta_Q = \frac{Q_2 - Q_1(p = p_h)}{Q_1(p = p_h)}, \quad (11)$$

and we note that $\Delta_Q = 0$ when $Q_1(p = p_h) = 0$.

Figure 14 shows Δ_Q for various (α, β) , for the fixed parameter set $(p_1, p_2; r) = (0.5, 1; 0.5)$. The black lines represent the boundaries between the LD/HD and MC phases of the single-species TASEP with hopping probability p_1 (boundary 1) and the single-species TASEP with $p = p_h$ (boundary 2). Therefore, the lower-left (upper-right) region beyond boundary 1 (boundary 2) corresponds to the LD/HD (MC) phases both for the two-species TASEP and for the single-species TASEP with $p = p_h$. This figure confirms that Δ_Q starts from 0 in the LD/HD phase, decreases, and finally yields to a constant value in the MC phase as (α, β) approaches the upper right.

Figure 15 plots Δ_Q as a function (p_1, p_2) for various $(\alpha, \beta) \in \{(0.1, 0.2), (0.2, 0.1), (1, 1)\}$, fixing $r = 0.5$. Note that both the single-species TASEP with hopping probability p_h and the two-species TASEP exhibit the LD, HD, and MC phases with $(\alpha, \beta) = (0.1, 0.2)$, $(0.2, 0.1)$, and $(1, 1)$, respectively. This is because $\forall (p_1, p_2)$ ($0.2 \leq p_1, p_2 \leq 1$) $0.1 < 1 - \sqrt{1 - p_{\min}} \leq 1 - \sqrt{1 - p_h}$. For example, Fig. 13 confirms that those three points exist within each corresponding phase for $(p_1, p_2) = (0.5, 1)$.

In Figs. 15 (a) and (b), we find that Δ_Q is approximately 0, whereas Δ_Q deviates from 0 in Fig. 15 (c),

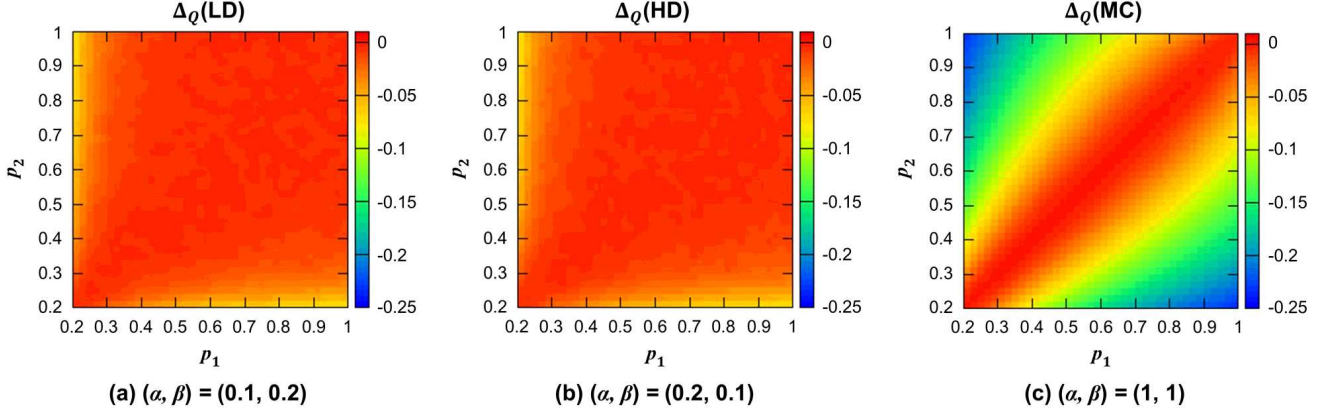


FIG. 15. (Color online) Calculated values of Δ_Q for various (p_1, p_2) , $S = 2$, and $r = 0.5$, (a) $(\alpha, \beta) = (0.1, 0.2)$ (LD), (b) $(\alpha, \beta) = (0.2, 0.1)$ (HD), and (c) $(\alpha, \beta) = (1, 1)$ (MC).

as is also observed in Fig. 14. These phenomena can be explained as follows.

First, in the LD/HD phase, Q_2 is mainly governed by the input/output probability, leading to $\Delta_Q \rightarrow 0$, i.e., Q_2 approaches $Q_1(p = p_h)$. This is because Q_2 deviates from $Q_1(p = p_h)$ mainly due to the existence of platoons, which do not influence the flow much in this phase. Note that Δ_Q decreases as α or β approaches 0.2, because the influence of platoons increases, approaching the MC phase of the two-species TASEP.

On the other hand, in the MC phase, Q_2 is mainly governed by the bulk region of the lattice. Therefore, the existence of platoons has a more critical influence on Q_2 , causing Δ_Q to deviate from 0; i.e., $Q_2 < Q_1(p = p_h)$. Especially as $|p_1 - p_2|$ increases, the extent of the deviation also increases. This is because the effect of platoons increases when there is a large gap between p_1 and p_2 .

B. Relation between T_R and T_G without the sorting cost

Hereafter, we assume $p_1 < p_2 < \dots < p_S$, $S > 1$, $\forall s$ $r_s > 0$, and $\alpha > 0$.

In this subsection, we fix $\lambda = 0$, i.e., we do not consider the sorting cost. If for any number of particle species s , $r_s N$ is large enough for T_G and T_R to be determined by the steady-state flow (see Appendix D), we obtain

$$T_R \approx \frac{N}{Q_S} \quad (12)$$

and

$$T_G \approx \sum_{s=1}^S \frac{r_s N}{Q_1(p = p_s)}. \quad (13)$$

Note that this approximation immediately implies the independence of T_G from the order of the group sequence.

Strictly speaking, T_G can differ depending on the order of each group in the group sequence. However, that difference can be ignored for large N (see Appendix D).

In addition, we define the transportation times of the particles with the same hopping probabilities p_h and p_{min} as

$$T_H \approx \frac{N}{Q_1(p = p_h)} \quad (14)$$

and

$$T_M \approx \frac{N}{Q_1(p = p_{min})}, \quad (15)$$

respectively. From Eqs. (9), (12), (14) and (15), we immediately obtain the inequality

$$T_H < T_R < T_M. \quad (16)$$

In the following, we show that a general relation between T_R and T_G can be obtained mathematically for general $S(> 1)$. We emphasize that this relation can be proven by comparing T_H and T_G , and not by comparing T_R and T_G directly. Here, we introduce the new function $f(\alpha, \beta; p_1, \dots, p_S; r_1, \dots, r_S)$, which is defined as follows:

$$f(\alpha, \beta; p_1, \dots, p_S; r_1, \dots, r_S) = T_H - T_G. \quad (17)$$

Because we can assume $\alpha < \beta$ without loss of generality, we adopt this assumption in the following discussion, writing in abbreviated form $f(\alpha, \beta; p_1, \dots, p_S; r_1, \dots, r_S) = f(\alpha)$. Note that for cases with $\alpha \geq \beta$, the theoretical results can be obtained simply by replacing α (LD) with β (HD).

A contour map of $f(\alpha)$ in the (α, β) plane exhibits four large regions, which are summarized in Tab. I.

In the following subsections, we examine the behavior of $f(\alpha)$ according to this classification.

TABLE I. Classification of Regions

Region No.	Range
1	$\alpha < 1 - \sqrt{1 - p_1}$
2	$1 - \sqrt{1 - p_1} \leq \alpha < 1 - \sqrt{1 - p_h}$
3	$1 - \sqrt{1 - p_h} \leq \alpha < 1 - \sqrt{1 - p_S}$
4	$1 - \sqrt{1 - p_S} \leq \alpha$

1. *Region 1:* $\alpha < 1 - \sqrt{1 - p_1}$

In this region, all the steady-state phases of the single-species TASEP for any p_s exhibit the LD phase. Here, the steady-state flow for the single-species TASEP with parallel updating [27] is given by

$$Q_1(p) = \begin{cases} \alpha \frac{p - \alpha}{p - \alpha^2} & \text{for LD phase.} \\ \frac{1}{2}(1 - \sqrt{1 - p}) & \text{for MC phase.} \end{cases} \quad (18)$$

Therefore, we obtain

$$T_G \approx \sum_{s=1}^S \frac{r_s N(p_s - \alpha^2)}{\alpha(p_s - \alpha)} \quad (19)$$

and

$$T_H \approx \frac{N(p_h - \alpha^2)}{\alpha(p_h - \alpha)}. \quad (20)$$

From Eqs.(19) and (20), we obtain $f(\alpha)$ as

$$f(\alpha) = \frac{N(p_h - \alpha^2)}{\alpha(p_h - \alpha)} - \sum_{s=1}^S \frac{r_s N(p_s - \alpha^2)}{\alpha(p_s - \alpha)}. \quad (21)$$

After some calculations, we obtain

$$f(\alpha) < 0; \quad (22)$$

the detailed derivation is given in Appendix E.

2. *Region 2:* $1 - \sqrt{1 - p_1} \leq \alpha < 1 - \sqrt{1 - p_h}$

This region is further divided into $(u - 1)$ subregions, as summarized in Tab. II.

In Subregion $2-v$ ($v = 1, 2, \dots, u - 1$), the single-species TASEP with $p = p_1, \dots, p_v, p_h$ exhibits the MC phase, whereas that with $p = p_{v+1}, \dots, p_S$ displays the LD phase. Therefore, using Eq. (18), we obtain

$$Q_1(p) = \begin{cases} \frac{1}{2}(1 - \sqrt{1 - p}) & \text{for } p = p_1, \dots, p_{v-1}, p_h. \\ \alpha \frac{p - \alpha}{p - \alpha^2} & \text{for } p = p_{v+1}, \dots, p_S. \end{cases} \quad (23)$$

From Eqs. (13), (14), and (23), T_G and T_H can be written as follows;

TABLE II. Classification of subregions in Region 2

Subregion No.	Range
2-1	$1 - \sqrt{1 - p_1} \leq \alpha < 1 - \sqrt{1 - p_2}$
2-2	$1 - \sqrt{1 - p_u} \leq \alpha < 1 - \sqrt{1 - p_{u+1}}$
...	...
2-v	$1 - \sqrt{1 - p_v} \leq \alpha < 1 - \sqrt{1 - p_{v+1}}$
...	...
2-(u-1)	$1 - \sqrt{1 - p_{u-1}} \leq \alpha < 1 - \sqrt{1 - p_h}$

$$T_G \approx \sum_{s=1}^v \frac{2r_s N}{1 - \sqrt{1 - p_s}} + \sum_{s=v+1}^S \frac{r_s N(p_s - \alpha^2)}{\alpha(p_s - \alpha)} \quad (24)$$

and

$$T_H \approx \frac{N(p_h - \alpha^2)}{\alpha(p_h - \alpha)}. \quad (25)$$

From Eqs. (24) and (25), we thus obtain $f(\alpha)$ in the form

$$f(\alpha) \approx \frac{N(p_h - \alpha^2)}{\alpha(p_h - \alpha)} - \sum_{s=1}^v \frac{2r_s N}{1 - \sqrt{1 - p_s}} - \sum_{s=v+1}^S \frac{r_s N(p_s - \alpha^2)}{\alpha(p_s - \alpha)}. \quad (26)$$

For $1 - \sqrt{1 - p_v} \leq \alpha < 1 - \sqrt{1 - p_{v+1}}$, due to $\alpha < p_{v+1} < \dots < p_S$ and $\alpha < p_h$, we obtain $p_s - \alpha > 0$ for $s = v + 1, \dots, S$ and $p_h - \alpha > 0$. The function $f(\alpha)$ is continuous and differentiable with respect to α , including at each boundary (see Appendix F). However, the signs of $f(\alpha)$ and $df(\alpha)/d\alpha$ are not specified. Note that the following condition

$$\lim_{\alpha \rightarrow q_h - 0} \frac{df(\alpha)}{d\alpha} > 0, \quad (27)$$

where $q_h = 1 - \sqrt{1 - p_h}$ indicates that $f(\alpha)$ increases monotonically at least near the boundary between Subregion $2-(u-1)$ and Region 3. This is discussed in Appendix G.

3. *Region 3:* $1 - \sqrt{1 - p_h} \leq \alpha < 1 - \sqrt{1 - p_S}$

Similarly to Region 2, this region is further divided into $(S - u + 1)$ subregions, as summarized in Tab. III. Note that Subregion $3-1$ vanishes in the case $p_h = p_u$, resulting in $(S - u)$ subregions.

In Region $3-v$ ($v = u, u + 1, \dots, S$), the single-species TASEP with $p = p_1, \dots, p_{v-1}, p_h$ exhibits the MC phase, whereas that with $p = p_v, \dots, p_S$ displays the LD phase. Therefore, using Eq. (18), we obtain $Q_1(p)$

$$Q_1(p) = \begin{cases} \frac{1}{2}(1 - \sqrt{1 - p}) & \text{for } p = p_1, \dots, p_{v-1}, p_h. \\ \alpha \frac{p - \alpha}{p - \alpha^2} & \text{for } p = p_v, \dots, p_S. \end{cases} \quad (28)$$

TABLE III. Classification of subregions in Region 3

Subregion No.	Range
3-u	$1 - \sqrt{1 - p_h} \leq \alpha < 1 - \sqrt{1 - p_u}$
3-(u+1)	$1 - \sqrt{1 - p_u} \leq \alpha < 1 - \sqrt{1 - p_{u+1}}$
...	...
3-v	$1 - \sqrt{1 - p_{v-1}} \leq \alpha < 1 - \sqrt{1 - p_v}$
...	...
3-S	$1 - \sqrt{1 - p_{S-1}} \leq \alpha < 1 - \sqrt{1 - p_S}$

From Eqs. (13), (14), and (28), T_G and T_H can be written as follows;

$$T_G \approx \sum_{s=1}^{v-1} \frac{2r_s N}{1 - \sqrt{1 - p_s}} + \sum_{s=v}^S \frac{r_s N(p_s - \alpha^2)}{\alpha(p_s - \alpha)} \quad (29)$$

and

$$T_H \approx \frac{2N}{1 - \sqrt{1 - p_h}}. \quad (30)$$

From Eqs. (29) and (30), $f(\alpha)$ becomes

$$f(\alpha) \approx \frac{2N}{1 - \sqrt{1 - p_h}} - \sum_{s=1}^{v-1} \frac{2r_s N}{1 - \sqrt{1 - p_s}} - \sum_{s=v}^S \frac{r_s N(p_s - \alpha^2)}{\alpha(p_s - \alpha)}. \quad (31)$$

For $1 - \sqrt{1 - p_{v-1}} \leq \alpha < 1 - \sqrt{1 - p_v}$, due to $\alpha < p_v < \dots < p_S$, we obtain $p_s - \alpha > 0$ for $s = v, \dots, S$. Similarly to Region 2, $f(\alpha)$ is continuous and differentiable with respect to α including at each boundary.

After some calculations, we find that $df(\alpha)/d\alpha$ satisfies

$$\frac{df(\alpha)}{d\alpha} > 0 \quad (32)$$

in each subregion, as discussed in detail in Appendix H. Eq. (32) indicates that $f(\alpha)$ is a monotonically increasing function of α throughout Region 3.

4. Region 4: $1 - \sqrt{1 - p_S} \leq \alpha$

In this region, all the steady-state phases of the single-species TASEP for any hopping probabilities p_s and p_h exhibit the MC region. Note that this region vanishes in the case $p_S = 1$ because $1 - \sqrt{1 - p_S} = 1$. Therefore, we obtain

$$T_G \approx \sum_{s=1}^S \frac{2r_s N}{1 - \sqrt{1 - p_s}} \quad (33)$$

and

$$T_H \approx \frac{2N}{1 - \sqrt{1 - p_h}}, \quad (34)$$

both of which are independent of α . From Eqs. (33) and (34), we thus obtain $f(\alpha)$ as

$$f(\alpha) = \frac{2N}{1 - \sqrt{1 - p_h}} - \sum_{s=1}^S \frac{2r_s N}{1 - \sqrt{1 - p_s}}. \quad (35)$$

After some calculations, we obtain

$$f(\alpha) > 0, \quad (36)$$

the detailed derivation of which is given in Appendix I.

5. Relation between T_R and T_G

With the results of Subsec. IV B 1–IV B 4, we can obtain a general relation between T_R and T_G for some special cases. Table IV summarizes the signs of $f(\alpha)$ and $df(\alpha)/d\alpha$ in each region. Note that ‘U’ indicates that the sign is unclear.

TABLE IV. Sign of $f(\alpha)$ and $df(\alpha)/d\alpha$

Region No.	$f(\alpha)$	$df(\alpha)/d\alpha$
1	–	U
2	U	U
3	U	+
4	+	0

Considering Tab. IV and the continuity of $f(\alpha)$ including at each boundary (see Appendix F), we find from the intermediate value theorem that $\exists \alpha_{cr}$ such that f satisfies

$$f(\alpha = \alpha_{cr}) = 0 \Leftrightarrow T_H = T_G \quad (37)$$

in Region 2 or 3. The specific conditions that α_{cr} must satisfy are given in Appendix J.

Defining $\alpha_{cr, \max}$ as the largest value among the quantities α_{cr} , we obtain $f(\alpha) > 0$ —i.e., $T_H > T_G$ —in the region where $\alpha > \alpha_{cr, \max}$. This is because $f(\alpha)$ is continuous and increases monotonically from a point in Region 2 (and through Region 3), to yield $f(\alpha) > 0$ in Region 4.

Considering Eq. (16), we finally obtain

$$T_G < T_H < T_R \quad (38)$$

in the region $\alpha > \alpha_{cr, \max}$. Eq. (38) means that $\Delta_T < 0$, reproducing the simulation results in the region where $\min(\alpha, \beta)$ is relatively large. This result indicates that the group-advantageous region must appear even in a case with $p_S = 1$, for which Region 4 vanishes.

In analogy with the discussion above, we can also predict that a region with $\Delta_T < 0$ must appear in the case $S = N$.

C. Relation between T_R and T_G with sorting cost

In this subsection, we discuss the change in the relation between T_R and T_G when $\lambda > 0$, i.e., when the sorting cost is included. In the following, we first obtain a general formula for the sorting cost and then evaluate upper and lower limits to λ .

1. General formula for the sorting cost

First, we calculate mathematically the averaged minimal number of exchanges necessary to sorting the particles from random to group sequences.

We here define \bar{K} as the averaged value of K , using the fact that τ_R can take $N! / \prod_{s=1}^S (r_s N)!$ patterns with equal probability. We thus have

$$\bar{K} = \frac{\prod_{s=1}^S (r_s N)!}{N!} \sum_{\forall \tau_R} K(\tau_G, \tau_R). \quad (39)$$

If $K'(\tau_G, \tau_R)$ is the minimal number of exchanges necessary to sort the particles from a random sequence τ_R to a given fixed group sequence τ_G , then $K'(\tau_G, \tau_R)$ satisfies

$$K'(\tau_G, \tau_R) = \min\{K(\tau_G, \tau_R)\}. \quad (40)$$

Note that the number of elements of $\{K(\tau_G, \tau_R)\}$ is equal to that of $\{\tau_G\}$ from the definition. Eqs. (39) and (40) indicate that the best group sequence τ_G can vary depending on the particular random sequence τ_R .

Due to the difficulty of a general calculation of \bar{K} , we instead calculate \bar{K}' , which is defined as follows:

$$\bar{K}' = \frac{\prod_{s=1}^S (r_s N)!}{N!} \sum_{\forall \tau_R} K'(\tau_G, \tau_R), \quad (41)$$

where τ_G is a fixed sequence out of the set $\{\tau_G\}$ for all possible τ_R .

For $S = 2$ and $S = N$, \bar{K}' can be generally calculated as

$$\bar{K}' = \begin{cases} r(1-r)N & \text{for } S = 2, \\ N - \sum_{k=1}^N \frac{1}{k} & \text{for } S = N, \end{cases} \quad (42)$$

the detailed derivations of which are discussed in Appendix K.

Figure 16 shows the ratio \bar{K}/\bar{K}' for (a) $S = 2$ and (b) $S = N$. Both figures show that $\bar{K}/\bar{K}' \approx 1$, i.e., $\bar{K} \approx \bar{K}'$, indicating that there is no problem in substituting \bar{K}' for \bar{K} for large enough N .

In the following calculations, we therefore use \bar{K}' instead of \bar{K} because \bar{K}' can be represented by a general formula, whereas \bar{K} cannot.

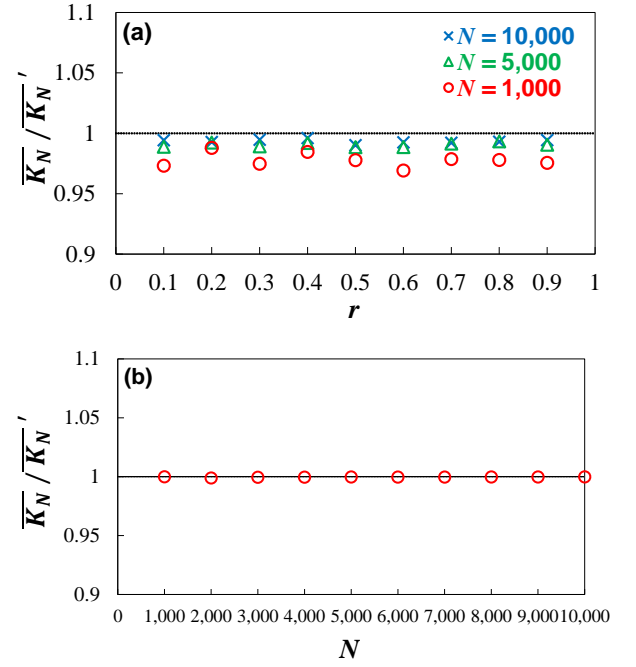


FIG. 16. (Color online) (a) Simulation values of \bar{K}/\bar{K}' for various $N \in \{1,000(\text{red}), 5,000(\text{green}), 10,000(\text{blue})\}$ for $S = 2$. (b) Simulation values of \bar{K}/\bar{K}' for $S = N$. Note that \bar{K} and \bar{K}' are each simulation values obtained by respectively averaging over 100 trials.

2. Upper and lower limits to λ_{cr}

We first define $\lambda = \lambda_{cr} \geq 0$, as the value for which $T_R = T_G$. Note that λ_{cr} is defined to be equal to 0 if $T_R \leq T_G$ when $\lambda = 0$. From the definition of λ_{cr} , the random-advantageous region appears when $\lambda > \lambda_{cr}$. Based on the discussions in Subsec. IV B and IV C 1, we here evaluate λ_{cr} for $S = 2$ and $\alpha < \beta$.

To take into account the sorting cost, we add the term λK ($\lambda > 0$) to T_G ; that is,

$$T_G \approx \lambda \bar{K}' + \sum_{s=1}^S \frac{r_s N}{Q_1(p = p_s)}. \quad (43)$$

Conversely, we do not add that term to T_R because a random sequence means a sequence without sorting.

We also define λ_H and λ_M as the values of λ for which $T_H = T_G$ and $T_M = T_G$, respectively. Note that λ_H can have negative values, because T_H can be less than T_G .

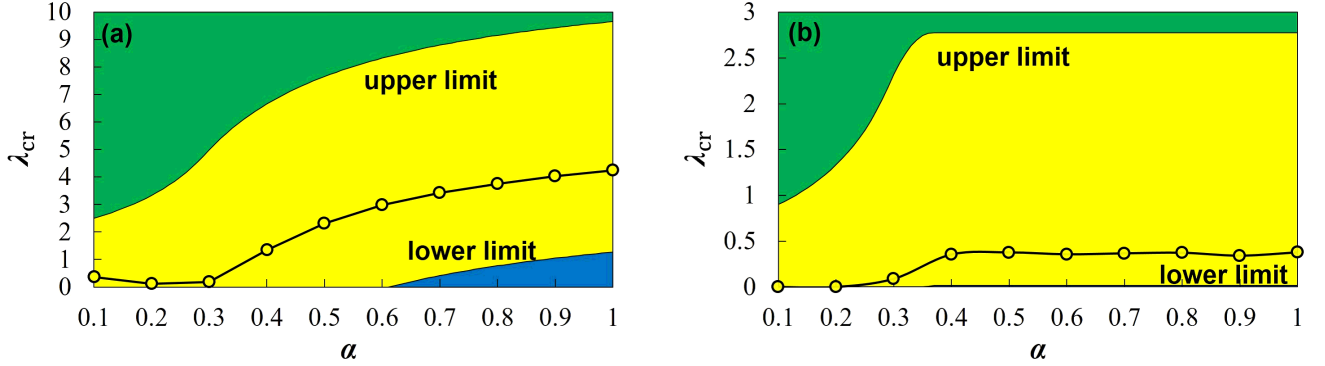
From Eq. (16) and Subsec. IV B, when $\lambda = 0$ the relations among T_R , T_G , T_H , and T_M must satisfy one of the following three inequalities:

$$T_H < T_R \leq T_G < T_M, \quad (44)$$

$$T_H < T_G < T_R < T_M, \quad (45)$$

TABLE VI. Upper and lower limits to λ_{cr}

Region No.	Upper and lower limits to λ_{cr}
1	$0 \leq \lambda < \frac{1}{r\alpha} \left(\frac{p_1 - \alpha^2}{p_1 - \alpha} - \frac{p_2 - \alpha^2}{p_2 - \alpha} \right)$
2	$\max \left\{ 0, \frac{1}{r(1-r)} \left(\frac{p_h - \alpha^2}{\alpha(p_h - \alpha)} - \frac{2r}{1 - \sqrt{1-p_1}} - \frac{(1-r)(p_2 - \alpha^2)}{\alpha(p_2 - \alpha)} \right) \right\} \leq \lambda_{\text{cr}} < \frac{1}{r} \left(\frac{2}{1 - \sqrt{1-p_1}} - \frac{p_2 - \alpha^2}{\alpha(p_2 - \alpha)} \right)$
3	$\max \left\{ 0, \frac{1}{r(1-r)} \left(\frac{2}{1 - \sqrt{1-p_h}} - \frac{2r}{1 - \sqrt{1-p_1}} - \frac{(1-r)(p_2 - \alpha^2)}{\alpha(p_2 - \alpha)} \right) \right\} \leq \lambda_{\text{cr}} < \frac{1}{r} \left(\frac{2}{1 - \sqrt{1-p_1}} - \frac{p_2 - \alpha^2}{\alpha(p_2 - \alpha)} \right)$
4	$\frac{2}{r(1-r)} \left(\frac{1}{1 - \sqrt{1-p_h}} - \frac{r}{1 - \sqrt{1-p_1}} - \frac{1-r}{1 - \sqrt{1-p_2}} \right) < \lambda_{\text{cr}} < \frac{2}{r} \left(\frac{1}{1 - \sqrt{1-p_1}} - \frac{1}{1 - \sqrt{1-p_2}} \right)$

FIG. 17. (Color online) Simulation values (black circles) and the theoretical existence range of λ_{cr} (yellow region) as functions of α . The other parameters are fixed at $(\beta; p_1, p_2; r) =$ (a) $(1; 0.5, 1; 0.5)$ and (b) $(1; 0.5, 0.6; 0.5)$.

or

$$T_G < T_H < T_R < T_M. \quad (46)$$

Therefore, the relations of λ_{cr} , λ_H , and λ_M can be written as follows:

$$\max(0, \lambda_H) \leq \lambda_{\text{cr}} < \lambda_M, \quad (47)$$

where we note that by definition $\lambda_{\text{cr}} \geq 0$, whereas λ_H can be either negative or positive, while λ_M must be positive.

In Region 1, i.e., $\alpha < 1 - \sqrt{1-p_1}$, where $T_H < T_G$ with $\lambda = 0$, λ_H must be negative, while λ_M must be positive, and satisfy

$$\begin{aligned} & \frac{N(p_1 - \alpha^2)}{\alpha(p_1 - \alpha)} \\ & \approx \lambda_M r(1-r)N + \frac{rN(p_1 - \alpha^2)}{\alpha(p_1 - \alpha)} + \frac{(1-r)N(p_2 - \alpha^2)}{\alpha(p_2 - \alpha)}. \end{aligned} \quad (48)$$

In Region 2, i.e., $1 - \sqrt{1-p_1} \leq \alpha < 1 - \sqrt{1-p_h}$, λ_H can be either negative or positive, whereas λ_M must be

positive. The quantities λ_H and λ_M satisfy

$$\begin{aligned} & \frac{rN(p_h - \alpha^2)}{\alpha(p_h - \alpha)} \\ & \approx \lambda_H r(1-r)N + \frac{2rN}{1 - \sqrt{1-p_1}} + \frac{(1-r)N(p_2 - \alpha^2)}{\alpha(p_2 - \alpha)} \end{aligned} \quad (49)$$

and

$$\begin{aligned} & \frac{2N}{1 - \sqrt{1-p_1}} \\ & \approx \lambda_M r(1-r)N + \frac{2rN}{1 - \sqrt{1-p_1}} + \frac{(1-r)N(p_2 - \alpha^2)}{\alpha(p_2 - \alpha)}, \end{aligned} \quad (50)$$

respectively.

In Region 3, i.e., $1 - \sqrt{1-p_h} \leq \alpha < 1 - \sqrt{1-p_2}$, λ_H can be either negative or positive, and λ_M must be positive. Thus, λ_H and λ_M satisfy

$$\begin{aligned} & \frac{2N}{1 - \sqrt{1-p_h}} \\ & \approx \lambda_H r(1-r)N + \frac{2rN}{1 - \sqrt{1-p_1}} + \frac{(1-r)N(p_2 - \alpha^2)}{\alpha(p_2 - \alpha)} \end{aligned} \quad (51)$$

and

$$\frac{2N}{1 - \sqrt{1 - p_1}} \approx \lambda_M r(1 - r)N + \frac{2rN}{1 - \sqrt{1 - p_1}} + \frac{(1 - r)N(p_2 - \alpha^2)}{\alpha(p_2 - \alpha)}, \quad (52)$$

respectively.

In Region 4, i.e., $1 - \sqrt{1 - p_2} \leq \alpha$, due to $T_G < T_H < T_M$ when $\lambda = 0$, λ_H and λ_M must both be positive. The quantities λ_H and λ_M therefore satisfy

$$\frac{2N}{1 - \sqrt{1 - p_h}} \approx \lambda_H r(1 - r)N + \frac{2rN}{1 - \sqrt{1 - p_1}} + \frac{2(1 - r)N}{1 - \sqrt{1 - p_2}} \quad (53)$$

and

$$\frac{2N}{1 - \sqrt{1 - p_1}} \approx \lambda_M r(1 - r)N + \frac{2rN}{1 - \sqrt{1 - p_1}} + \frac{2(1 - r)N}{1 - \sqrt{1 - p_2}}, \quad (54)$$

respectively.

Table VI summarizes the upper and lower limits to λ_{cr} in each region. Furthermore, Fig. 17 shows the simulation values (black circles) and the theoretical existence range of λ_{cr} (yellow region) as functions of α . Note that the we calculated the simulation values using with 10-trial-averaged values of T_R , T_G , and K .

We can interpret Fig. 17 as demonstrating that a group (random) sequence is preferable in the region below (above) the black line. In the blue (green) region, a group (random) sequence is in fact theoretically verified to be preferable. Comparing Figs. 17 (a) and (b), the simulation values approach the lower limit—i.e., the accuracy of approximating T_R by T_H increases—as $|p_1 - p_2|$ decreases. We admit that the yellow region is extensive, especially when $|p_1 - p_2|$ is relatively large; however, we emphasize that the simulation values always exist within the expected region and that the region can be limited easily without numeric calculations, which is convenient for applications to actual situations.

V. CONCLUSION

In the present paper, we have used a modified TASEP to analyze the dependence of the transportation time on the entering sequences of particles, using both the numerical simulations and theoretical analyses.

Here, we summarize a number of important results. In Sec. III, we discovered that there exists an important ‘group-advantageous region’ where $T_R > T_G$ when $\min(\alpha, \beta)$ is relatively large and the sorting costs are neglected. When sorting costs are introduced, a new region called a ‘random-advantageous region’ appears with

$T_R < T_G$. In addition, the group-advantageous region shrinks and finally disappears as λ increases. We explored these phenomena for various $S \in \{2, 3, N\}$.

In Sec. IV, we analyzed the simulation results by employing mathematical approaches for certain special cases. Using some approximations, we have shown theoretically that without the sorting cost the group-advantageous region must appear for any parameter sets (S, p_s, r_s) . Moreover, we have succeeded in deriving the upper and lower limits to the value of λ_{cr} where $T_R = T_G$ by obtaining a general formula for the sorting cost.

Our proposed method can be interpreted as providing smooth logistics for various products and as yielding an effective evacuation method for pedestrians in various situations. For example, we can determine whether or not the bunching of products (pedestrians) with almost the same size (velocity) should be implemented before transportation, depending upon the magnitude of the bunching cost.

ACKNOWLEDGMENTS

This work was partially supported by JST-Mirai Program Grant Number JPMJMI17D4, Japan, JSPS KAKENHI Grant Number JP15K17583, and MEXT as gPost-K Computer Exploratory Challengesh (Exploratory Challenge 2: Construction of Models for Interaction Among Multiple Socioeconomic Phenomena, Model Development and its Applications for Enabling Robust and Optimized Social Transportation Systems) (Project ID: hp180188).

Appendix A: Validity of our selection of L and N

In this Appendix, we briefly discuss the validity of selecting $L = 200$ and $N = 10,000$.

As finite-size effects may occur for small L , we compare the simulation values of Q_2 for $L = 200$ and $L = 1,000$. Figure 18 shows the ratio Q_2/Q'_2 , where Q_2 and Q'_2 represent the flow of the multi-species TASEP with $L = 200$ and $L = 1,000$, respectively, as functions of α for various $\beta \in \{0.2, 0.6, 1\}$. The result that $Q_2/Q'_2 \approx 1$ indicates that the effect can be ignored for $L = 200$. Thus, we choose $L = 200$ to decrease the simulation time.

On the other hand, the assumption that T is determined by a steady-state flow may be inappropriate for small N . Therefore, we have compared the results for $N = 10,000$ and $N = 20,000$, in both cases for $L = 200$. Figure 19 shows the ratio T/T' , where T and T' represent the transportation times for $N = 10,000$ and $N = 20,000$, respectively, as functions of α for various $\beta \in \{0.2, 0.6, 1\}$. The result that $T/T' \approx 0.5$, i.e., that T is proportional to N , indicates that the assumption can be regarded as valid for $N = 10,000$. Thus, we choose $N = 10,000$ similarly to decrease the simulation time.

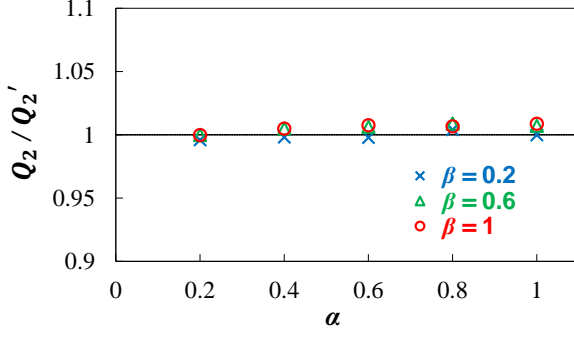


FIG. 18. (Color online) Simulation values of the ratio Q_2/Q_2' as a function of α for various $\beta \in \{0.2, 0.6, 1\}$. The other parameters are fixed at $(p_1, p_2; r) = (0.5, 1; 0.5)$.

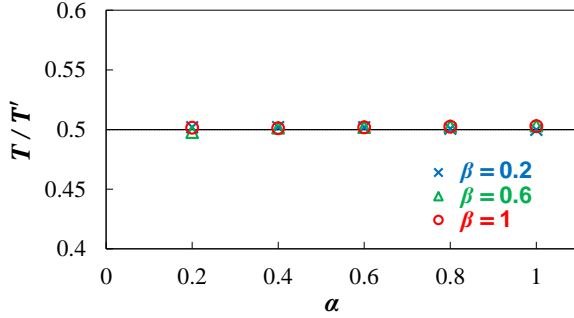


FIG. 19. (Color online) Simulation values of T/T' as a function of α for various $\beta \in \{0.2, 0.6, 1\}$. The other parameters are fixed at $L = 200$ and $(p_1, p_2; r) = (0.5, 1; 0.5)$.

Appendix B: Simulation schemes for obtaining the minimal number of necessary exchanges

In this Appendix, we briefly describe the specific simulation schemes we used to obtain K . We emphasize that the cost of counting or comparing particles and the distances between exchanged particles are both ignored in the following.

First, for $S = 2$, $\tau_a = \tau_G$ can have only one of two patterns. Once τ_G is fixed to be either of these two sequences, we can immediately obtain the number of particles placed at the wrong areas in sequence $\tau_b = \tau_R$, which is twice as large as the number of necessary exchanges (see also Appendix K). Consequently, comparing the results for the two τ_G gives the smaller number as K .

Second, for $S = 3$, $\tau_a = \tau_G$ can have six patterns. Once τ_G is fixed at one of these six sequences, we can immediately obtain the number of particles placed at the wrong areas in any sequence $\tau_b = \tau_R$. After selecting one species, which we first replace at the correct location, we exchange all particles of that species that are placed in the wrong areas in sequence $\tau_b = \tau_R$. The subsequent procedure is similar to the case for $S = 2$. Conse-

quently, comparing the six results for each τ_G again gives the smallest number as K . Note that we can similarly calculate the numbers for general $S > 4$.

Finally, for $S = N$, $\tau_a = \tau_G$ can have one of two patterns: either an ascending or a descending sequence. One exchange is needed for each particle in $\tau_b = \tau_R$ for which there exists a particle with a smaller (larger) hopping probability than the noted particle. This is termed a ‘selection sort.’ This procedure starts from the leading particle. Consequently, by comparing the results for the two τ_G , the smaller number is again selected as the minimal number of necessary exchanges.

Appendix C: Approximate Q_S for general S with $L = 2$

In this Appendix, we prove the proposition that the S -species TASEP is equivalent to the single-species TASEP with hopping probability p_h for $L = 2$ by using mathematical induction.

Assume that this proposition is true for $S = k$; that is, that k -species TASEP is equivalent to the single-species TASEP with hopping probability p_h , i.e., with the harmonic mean of $\{p_1, p_2, \dots, p_k\}$. Note that p_h can be written as

$$p_h = \frac{1}{\sum_{s=1}^k r_s/p_s}, \quad (\text{C1})$$

where

$$\sum_{s=1}^k r_s = 1. \quad (\text{C2})$$

Now, given that the assumption holds for $S = k$, the $(k+1)$ -species TASEP can be regarded as equivalent to the two-species TASEP with $p'_1 = p_h$ and $p'_2 = p_{k+1}$, where the fractions of two particle species are $r'_1 = 1 - r_{k+1}$ and $r'_2 = r_{k+1}$, respectively. From the results of Subsec. IV A 1, the two-species TASEP is proved to be equivalent to the single-species TASEP with $p = p'_h$, which can be written as

$$\begin{aligned} p'_h &= \frac{1}{r'_1/p'_1 + r'_2/p'_2} \\ &= \frac{1}{(1 - r_{k+1})/p_h(k) + r_{k+1}/p_{k+1}}. \end{aligned} \quad (\text{C3})$$

Substituting Eqs. (C1) and (C2) into the denominator of Eq. (C3), we obtain

$$\begin{aligned}
& \frac{1 - r_{k+1}}{p_h(k)} + \frac{r_{k+1}}{p_{k+1}} \\
&= (1 - r_{k+1}) \sum_{s=1}^k \frac{r_s}{p_s} + \frac{r_{k+1}}{p_{k+1}} \\
&= \sum_{s=1}^k \frac{r_s(1 - r_{k+1})}{p_s} + \frac{r_{k+1}}{p_{k+1}} \\
&= \sum_{s=1}^{k+1} \frac{r_s''}{p_s},
\end{aligned} \tag{C4}$$

where

$$r_s'' = \begin{cases} r_s(1 - r_{k+1}) & \text{for } s = 1, 2, \dots, k. \\ r_{k+1} & \text{for } s = k + 1. \end{cases} \tag{C5}$$

Note that r_s'' satisfies $\sum_{s=1}^{k+1} r_s'' = 1$ and can take all possible values between 0 and 1 ($0 < r_s'' < 1$) with proper choice of r_s ($s = 1, 2, \dots, k$) and r_{k+1} . Therefore, the proposition is true for $S = k + 1$.

The case $S = 2$ satisfies this proposition as we proved in Subsec. IV A 1.

The proposition is consequently true for every natural number S , yielding

$$Q_S = Q_1(p = p_h) = Q_1 \left(p = \frac{1}{\sum_{s=1}^S r_s/p_s} \right). \tag{C6}$$

Appendix D: Validity of the approximation for T

In this Appendix, we briefly demonstrate the validity of Eq. (13).

Figure 20 (a) shows the ratio $T_{G,\text{sim}}/T_{G,\text{theo}}$ as a function of α for various $\beta \in \{0.2, 0.6, 1\}$ with $S = 2$ and Fig. 20 (b) shows the same ratio for $S = 3$. Note that $T_{G,\text{sim}}$ and $T_{G,\text{theo}}$ represent the values of T_G from the simulations and that given by Eq. (13), respectively. Both figures show that $T_{G,\text{sim}}/T_{G,\text{theo}} \approx 1$, indicating that Eq. (13) provides a good approximation for T_G .

Strictly speaking, $T_{G,\text{sim}}/T_{G,\text{theo}}$ must be larger than 1 on average. This is mainly due to the fact that $T_{G,\text{sim}}$ includes T_1 , which is the time required for the first particle to reach the right-hand boundary, whereas $T_{G,\text{theo}}$ ignores that time. This also indicates that T_G can differ depending on the order of each group in the group sequence (i.e., the hopping probability of the leading group). However, this difference has little influences on the theoretical results, as explained below.

First, T_1 can be estimated as

$$T_1 \approx \frac{L}{p_s}, \tag{D1}$$

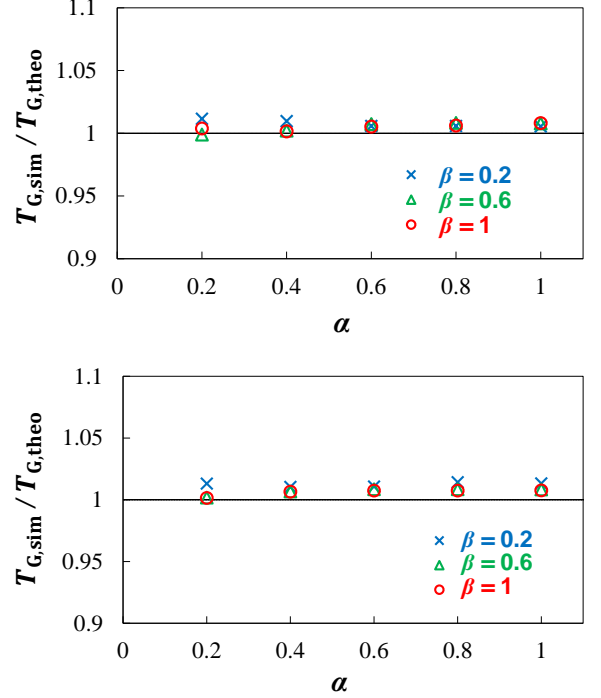


FIG. 20. (Color online) The ratio $T_{G,\text{sim}}/T_{G,\text{theo}}$ as a function of α for various $\beta \in \{0.2, 0.6, 1\}$ with (a) $S = 2$ and (b) $S = 3$. The other parameters are fixed at (a) $(p_1, p_2; r) = (0.5, 1; 0.5)$ and (b) $(p_1, p_2, p_3; r_1, r_2, r_3) = (0.4, 0.6, 0.8; 0.2, 0.3, 0.5)$.

where $s = 1, 2, \dots, S$ and the time steps before the first particle enters the lattice are assumed to be small enough to be ignored. The quantities T_1 and T_G without T_1 satisfy

$$T_1 \approx \frac{L}{p_s} < \frac{L}{p_S} < \frac{L}{1 - \sqrt{1 - p_S}} \tag{D2}$$

and

$$T_G \approx \sum_{s=1}^S \frac{r_s N}{Q_1(p = p_s)} > \frac{2N}{1 - \sqrt{1 - p_S}}, \tag{D3}$$

respectively. Therefore, T_1/T_G reduces to

$$\frac{T_1}{T_G} < \frac{L}{2N}. \tag{D4}$$

Under the proposition that N is large enough, we can assume $L/2N \ll 1$ ($L/2N = 0.01$ in the present paper). Moreover, all the times T (T_R , T_H , and T_M) originally include T_1 , so that this term disappears when they are subtracted from each other. Consequently, T_1 (and therefore, the dependence of T_G on the order of each group in the group sequence) can be assumed to be ignorable.

Appendix E: Discussion of the sign of $f(\alpha)$

in Region 1

In this Appendix, we give a detailed derivation of Eq. (22) for Region 1, where $\alpha < 1 - \sqrt{1 - p_1}$.

Eq. (21) gives $f(\alpha)$

$$\begin{aligned} f(\alpha) &= \frac{N(p_h - \alpha^2)}{\alpha(p_h - \alpha)} - \sum_{s=1}^S \frac{r_s N(p_s - \alpha^2)}{\alpha(p_s - \alpha)} \\ &= \frac{N}{\alpha} \sum_{s=1}^S \left\{ \frac{r_s(p_h - \alpha^2)}{p_h - \alpha} - \frac{r_s(p_s - \alpha^2)}{p_s - \alpha} \right\} \quad (\text{E1}) \\ &= \frac{N(\alpha - 1)}{(p_h - \alpha) \prod_{s=1}^S (p_s - \alpha)} C, \end{aligned}$$

where

$$C = \sum_{s=1}^S \left\{ r_s(p_h - p_s) \prod_{k \neq s} (p_k - \alpha) \right\}. \quad (\text{E2})$$

The quantity C is calculated as follows:

$$\begin{aligned} C &= \sum_{s=1}^S \left\{ r_s \left(\frac{1}{\sum_{t=1}^S r_t/p_t} - p_s \right) \prod_{k \neq s} (p_k - \alpha) \right\} \\ &= \frac{1}{D} \sum_{s=1}^S \left\{ r_s \left(\prod_{k=1}^S p_k - p_s \sum_{t=1}^S r_t \prod_{k \neq t} p_k \right) \prod_{k \neq s} (p_k - \alpha) \right\} \\ &= \frac{1}{D} \sum_{s=1}^S \sum_{t=1}^S \left\{ r_s r_t \left(\prod_{k=1}^S p_k - p_s \prod_{k \neq t} p_k \right) \prod_{k \neq s} (p_k - \alpha) \right\} \\ &= \frac{1}{D} \sum_{s=1}^S \sum_{t \neq s} \left\{ r_s r_t (p_t - p_s) \prod_{k \neq t} p_k \prod_{k \neq s} (p_k - \alpha) \right\}, \quad (\text{E3}) \end{aligned}$$

where

$$D = \sum_{s=1}^S \left(r_s \prod_{k \neq s} p_k \right). \quad (\text{E4})$$

By regarding the sum of the term with $(s, t) = (x, y)$ and that with $(s, t) = (y, x)$ as a new term for $\exists(x, y)$ ($x, y = 1, 2, \dots, S, x < y$), we can rewrite Eq. (E3) as follows:

$$\begin{aligned} C &= \frac{1}{D} \sum_{s=1}^S \sum_{t < s} \left\{ r_s r_t (p_t - p_s) \prod_{k \neq t} p_k \prod_{k \neq s} (p_k - \alpha) \right. \\ &\quad \left. + r_t r_s (p_s - p_t) \prod_{k \neq s} p_k \prod_{k \neq t} (p_k - \alpha) \right\} \\ &= \frac{1}{D} \sum_{s=1}^S \sum_{t < s} \left\{ \alpha r_s r_t (p_t - p_s)^2 \prod_{k \neq s, t} p_k \prod_{k \neq s, t} (p_k - \alpha) \right\}. \quad (\text{E5}) \end{aligned}$$

Because $p_s - \alpha > 0$ ($\forall s$) and $p_h - \alpha > 0$, we obtain $C > 0$.

Considering $\alpha - 1 < 0$ and $C > 0$, we finally obtain

$$f(\alpha) < 0. \quad (\text{E6})$$

Appendix F: Continuity and differentiability of $f(\alpha)$ at each boundary

In this Appendix, we briefly discuss the continuity and differentiability of $f(\alpha)$ at each boundary.

Defining $g(x)$ for $0 < x \leq 1$ as

$$g(x) = \begin{cases} \frac{p - x^2}{x(p - x)} & \text{for } 0 < x \leq 1 - \sqrt{1 - p}, \\ \frac{2}{1 - \sqrt{1 - p}} & \text{for } 1 - \sqrt{1 - p} < x \leq 1, \end{cases} \quad (\text{F1})$$

where $0 < p \leq 1$, the following equations hold:

$$\lim_{x \rightarrow q-0} g(x) = \lim_{x \rightarrow q+0} g(x) = \frac{2}{1 - \sqrt{1 - p}} \quad (\text{F2})$$

and

$$\lim_{\delta \rightarrow -0} \frac{g(x + \delta) - g(x)}{\delta} = \lim_{\delta \rightarrow +0} \frac{g(x + \delta) - g(x)}{\delta} = 0, \quad (\text{F3})$$

where $q = 1 - \sqrt{1 - p}$. Therefore, $g(x)$ is continuous and differentiable at $x = q = 1 - \sqrt{1 - p}$, resulting in the continuity and differentiability of $g(x)$ for $0 < x \leq 1$.

As a result, because $f(\alpha)$ is represented as a linear sum of terms $g(\alpha)$, where p is substituted for p_s or p_h ($0 < p_s, p_h \leq 1$), $f(\alpha)$ is clearly continuous and differentiable at each boundary.

Appendix G: Discussion of the sign of $df(\alpha)/d\alpha$ in Subregion 2-v

In this Appendix, we discuss the sign of $df(\alpha)/d\alpha$ in Subregion 2-v, i.e., $1 - \sqrt{1 - p_v} \leq \alpha < 1 - \sqrt{1 - p_{v+1}}$

From Eq. (26), $df(\alpha)/d\alpha$ can be calculated as follows:

$$\begin{aligned} \frac{df(\alpha)}{d\alpha} &\approx \frac{N(2\alpha - \alpha^2 - p_h)}{\alpha^2(p_h - \alpha)^2} - \sum_{s=u}^S \frac{r_s N(2\alpha - \alpha^2 - p_s)}{\alpha^2(p_s - \alpha)^2} \\ &= \sum_{s=1}^v \frac{r_s N(2\alpha - \alpha^2 - p_h)}{\alpha^2(p_h - \alpha)^2} \\ &\quad + \sum_{s=v+1}^S \left\{ \frac{r_s N(2\alpha - \alpha^2 - p_h)}{\alpha^2(p_h - \alpha)^2} - \frac{r_s N(2\alpha - \alpha^2 - p_s)}{\alpha^2(p_s - \alpha)^2} \right\} \\ &= \sum_{s=1}^v \frac{r_s N(2\alpha - \alpha^2 - p_h)}{\alpha^2(p_h - \alpha)^2} \\ &\quad + \sum_{s=v+1}^S \frac{r_s N(p_s - p_h) \{(\alpha - 1)^2 + p_s + p_h - p_s p_h - 1\}}{p_h p_s (p_h - \alpha)^2 (p_s - \alpha)^2}. \quad (\text{G1}) \end{aligned}$$

For $1 - \sqrt{1 - p_v} \leq \alpha < 1 - \sqrt{1 - p_{v+1}}$, the following two

inequalities hold:

$$\begin{aligned} & 2\alpha - \alpha^2 - p_h \\ & < 2(1 - \sqrt{1 - p_{v+1}}) - (1 - \sqrt{1 - p_{v+1}})^2 - p_h \quad (\text{G2}) \\ & = p_{v+1} - p_h < 0 \end{aligned}$$

and

$$\begin{aligned} & (\alpha - 1)^2 + p_s + p_h - p_s p_h - 1 \\ & > (1 - \sqrt{1 - p_{v+1}} - 1)^2 + p_s + p_h - p_s p_h - 1 \\ & > (1 - \sqrt{1 - p_h} - 1)^2 + p_s + p_h - p_s p_h - 1 \\ & = p_s(1 - p_h) > 0. \end{aligned} \quad (\text{G3})$$

We cannot specify the sign of $df(\alpha)/d\alpha$ in this subregion from Eqs. (G1), (G2), and (G3). However, near the boundary between Subregion 2-($u-1$) and 3- u , we obtain the following conditions:

$$\begin{aligned} & \lim_{\alpha \rightarrow q_h - 0} (2\alpha - \alpha^2 - p_h) \\ & = 2(1 - \sqrt{1 - p_h}) - (1 - \sqrt{1 - p_h})^2 - p_h = 0 \end{aligned} \quad (\text{G4})$$

and

$$\begin{aligned} & \lim_{\alpha \rightarrow q_h - 0} \{(\alpha - 1)^2 + p_s + p_h - p_s p_h - 1\} \\ & = (1 - \sqrt{1 - p_h} - 1)^2 + p_{u-1} + p_h - p_{u-1} p_h - 1 \quad (\text{G5}) \\ & = p_{u-1}(1 - p_h) > 0, \end{aligned}$$

where $q_h = 1 - \sqrt{1 - p_h}$. Therefore, noting the obvious continuity of $df(\alpha)/d\alpha$ for $1 - \sqrt{1 - p_v} \leq \alpha < 1 - \sqrt{1 - p_{v+1}}$, the region of $df(\alpha)/d\alpha > 0$ must exist at least in Subregion 2-($u-1$).

Appendix H: Discussion of the sign of $df(\alpha)/d\alpha$ in Subregion 3- v

In this Appendix, we give a proof on Eq. (32) in Subregion 3- v , i.e., $1 - \sqrt{1 - p_{v-1}} \leq \alpha < 1 - \sqrt{1 - p_v}$.

From Eq. (31), $df(\alpha)/d\alpha$ can be calculated as follows:

$$\frac{df(\alpha)}{d\alpha} \approx \sum_{s=v}^S \frac{r_s N(p_s - 2\alpha + \alpha^2)}{\alpha^2(p_s - \alpha)^2}. \quad (\text{H1})$$

For $s = v, \dots, S$, the quantity $p_s - 2\alpha + \alpha^2$ satisfies

$$\begin{aligned} & p_s - 2\alpha + \alpha^2 \\ & > p_s - 2(1 - \sqrt{1 - p_v}) + (1 - \sqrt{1 - p_v})^2 \quad (\text{H2}) \\ & = p_s - p_v > 0. \end{aligned}$$

From Eqs. (H1) and (H2), we finally obtain

$$\frac{df(\alpha)}{d\alpha} > 0. \quad (\text{H3})$$

Appendix I: Discussion of the sign of $f(\alpha)$ in Region 4

In this Appendix, we give a detailed derivation of Eq. (36), where $1 - \sqrt{1 - p_S} \leq \alpha$.

From Eqs. (33) and (34), $f(\alpha)$ can be represented as follows:

$$\begin{aligned} T_G & \approx 2N \sum_{s=1}^S \frac{r_s(1 + \sqrt{1 - p_s})}{p_s} \\ & = \frac{2N}{\prod_{s=1}^S p_s} \left\{ \sum_{s=1}^S (r_s + r_s \sqrt{1 - p_s}) \prod_{t \neq s} p_t \right\} \\ & = \frac{2N}{\prod_{s=1}^S p_s} \left\{ \sum_{s=1}^S \left(r_s \prod_{t \neq s} p_t \right) \right. \\ & \quad \left. + \sum_{s=1}^S \left(r_s \sqrt{1 - p_s} \prod_{t \neq s} p_t \right) \right\} \end{aligned} \quad (\text{I1})$$

and

$$\begin{aligned} T_H & \approx 2N \frac{1 + \sqrt{1 - p_h}}{p_h} \\ & = 2N \frac{1 + \sqrt{1 - 1/\sum_{s=1}^S (r_s/p_s)}}{1/\sum_{s=1}^S (r_s/p_s)} \\ & = \frac{2N}{\prod_{s=1}^S p_s} \left\{ \sum_{s=1}^S \left(r_s \prod_{t \neq s} p_t \right) \right. \\ & \quad \left. + \sqrt{\left(\sum_{s=1}^S r_s \prod_{t \neq s} p_t \right)^2 - \prod_{s=1}^S p_s \times \left(\sum_{s=1}^S r_s \prod_{t \neq s} p_t \right)} \right\} \end{aligned} \quad (\text{I2})$$

From Eqs. (35), (I1) and (I2), $f(\alpha)$ is given by

$$\begin{aligned} f(\alpha) & \approx \frac{2N}{\prod_{s=1}^S p_s} \left\{ \sqrt{\left(\sum_{s=1}^S r_s \prod_{t \neq s} p_t \right)^2 - \prod_{s=1}^S p_s \times \left(\sum_{s=1}^S r_s \prod_{t \neq s} p_t \right)} \right. \\ & \quad \left. - \sum_{s=1}^S \left(r_s \sqrt{1 - p_s} \prod_{t \neq s} p_t \right) \right\} \\ & = \frac{2N}{\prod_{s=1}^S p_s} (E - F), \end{aligned} \quad (\text{I3})$$

where

$$E = \sqrt{\left(\sum_{s=1}^S r_s \prod_{t \neq s} p_t \right)^2 - \prod_{s=1}^S p_s \times \left(\sum_{s=1}^S r_s \prod_{t \neq s} p_t \right)} \quad (\text{I4})$$

and

$$F = \sum_{s=1}^S \left(r_s \sqrt{1-p_s} \prod_{t \neq s} p_t \right). \quad (I5)$$

From Eqs. (I4) and (I5), $E^2 - F^2$ becomes

$$\begin{aligned} E^2 - F^2 &= \left(\sum_{s=1}^S r_s \prod_{t \neq s} p_t \right)^2 - \prod_{s=1}^S p_s \times \left(\sum_{s=1}^S r_s \prod_{t \neq s} p_t \right) \\ &\quad - \left\{ \sum_{s=1}^S \left(r_s \sqrt{1-p_s} \prod_{t \neq s} p_t \right) \right\}^2 \\ &= \sum_{s=1}^S \left(r_s \prod_{t \neq s} p_t \right)^2 - \sum_{s=1}^S \sum_{t \neq s} \left\{ r_s r_t \prod_{k \neq s} p_k \prod_{l \neq t} p_l \right\} \\ &\quad - \prod_{s=1}^S p_s \times \left(\sum_{s=1}^S r_s \prod_{t \neq s} p_t \right) \\ &\quad - \sum_{s=1}^S \left(r_s \prod_{t \neq s} p_t \right)^2 + \sum_{s=1}^S \left\{ r_s^2 p_s \left(\prod_{t \neq s} p_t \right)^2 \right\} \\ &\quad - \sum_{s=1}^S \sum_{t \neq s} \left\{ r_s r_t \sqrt{1-p_s} \sqrt{1-p_t} \prod_{k \neq s} p_k \prod_{l \neq t} p_l \right\} \\ &= \sum_{s=1}^S \left\{ \sum_{t \neq s} r_s r_t \prod_{k \neq s} p_k \prod_{l \neq t} p_l \right. \\ &\quad \left. - r_s (1-r_s) p_t \prod_{k \neq s} p_k \prod_{l \neq t} p_l \right. \\ &\quad \left. - \sum_{t \neq s} \left(r_s r_t \sqrt{1-p_s} \sqrt{1-p_t} \prod_{k \neq s} p_k \prod_{l \neq t} p_l \right) \right\} \\ &= \sum_{s=1}^S \sum_{t \neq s} \left[r_s r_t \prod_{k \neq s} p_k \prod_{l \neq t} p_l \times \right. \\ &\quad \left. \left\{ 1 - p_t - \sqrt{(1-p_s)(1-p_t)} \right\} \right]. \end{aligned} \quad (I6)$$

Here, regarding the sum of the term with $(s, t) = (x, y)$ and that with $(s, t) = (y, x)$ as a new term for $\exists(x, y) \ (x, y = 1, 2, \dots, S, x < y)$, Eq. (I6) can be rewritten as

ten as

$$\begin{aligned} E^2 - F^2 &= \sum_{s=1}^S \sum_{t < s} \left[r_s r_t \prod_{k \neq s} p_k \prod_{l \neq t} p_l \times \right. \\ &\quad \left. \left\{ 2 - p_s - p_t - \sqrt{(1-p_s)(1-p_t)} \right\} \right] \\ &= \sum_{s=1}^S \sum_{t < s} \left\{ r_s r_t \left(\sqrt{1-p_s} - \sqrt{1-p_t} \right)^2 \prod_{k \neq s} p_k \prod_{l \neq t} p_l \right\}. \end{aligned} \quad (I7)$$

Due to Eq. (I7) and the non-negativity of both E and F , we have $E > F$, thereby resulting in

$$f(\alpha) > 0. \quad (I8)$$

Appendix J: Specific conditions on $\alpha_{\text{cr}, \text{max}}$

Here, we discuss the specific conditions on $\alpha_{\text{cr}, \text{max}}$.

Table VI summarizes explicit expressions for $f(\alpha = \alpha_{\text{cr}}) = 0$, where the upper (lower) expression holds in Region 2 (Region 3). For $S = 2$, the lower expression becomes a quadratic equation in α_{cr} . However, the upper expression becomes a quartic equation that is too difficult to solve analytically those conditions. Note that for $S > 2$, both equations become more than quartic.

From its definition of $\alpha_{\text{cr}, \text{max}}$, $\alpha_{\text{cr}, \text{max}}$ can be written as

$$\alpha_{\text{cr}, \text{max}} = \max\{\alpha_{\text{cr}}\}, \quad (J1)$$

where $\{\alpha_{\text{cr}}\}$ represents the set of α_{cr} .

Appendix K: Derivation of \overline{K}'

In this Appendix, we derive the approximate averaged minimal number of exchanges \overline{K}' necessary to sort the particles for two special cases: $S = 2$ and $S = N$.

1. $S = 2$

First, for a general calculation of \overline{K}' , τ_{G} has to be fixed to be either of the two possible patterns. Once τ_{G} is fixed, $K(\tau_{\text{G}}, \tau_{\text{R}})$ can be determined uniquely for all possible τ_{R} . Without loss of generality, we can assume $rN \leq (1-r)N$ and τ_{G} can be fixed as illustrated in the lower panel of Fig. 21.

Suppose that for τ_{R} , k ($0 \leq k \leq rN$) particles of species 1 are located in the Area 2, (k particles of species 2 is located in the Area 1, conversely) as described in the lower of Fig. 21. Under this supposition, k -time exchanges are necessary for sorting particles from τ_{R} to τ_{G} .

TABLE VI. Explicit expressions for $f(\alpha = \alpha_{\text{cr}}) = 0$

Region No.	Explicit expressions for $f(\alpha = \alpha_{\text{cr}}) = 0$
2	$\frac{N(p_h - \alpha_{\text{cr}}^2)}{\alpha_{\text{cr}}(p_h - \alpha_{\text{cr}})} - \sum_{s=1}^v \frac{2r_s N}{1 - \sqrt{1 - p_s}} - \sum_{s=v+1}^S \frac{r_s N(p_s - \alpha_{\text{cr}}^2)}{\alpha_{\text{cr}}(p_s - \alpha_{\text{cr}})} = 0$ $\wedge \begin{cases} 1 - \sqrt{1 - p_v} < \alpha_{\text{cr}} < 1 - \sqrt{1 - p_{v+1}} & \text{for } 1 \leq v \leq u - 2 \\ 1 - \sqrt{1 - p_v} < \alpha_{\text{cr}} < 1 - \sqrt{1 - p_h} & \text{for } v = u - 1 \end{cases}$
3	$\frac{2N}{1 - \sqrt{1 - p_h}} - \sum_{s=1}^{v-1} \frac{2r_s N}{1 - \sqrt{1 - p_s}} - \sum_{s=v}^S \frac{r_s N(p_s - \alpha_{\text{cr}}^2)}{\alpha_{\text{cr}}(p_s - \alpha_{\text{cr}})} = 0$ $\wedge \begin{cases} 1 - \sqrt{1 - p_h} < \alpha_{\text{cr}} < 1 - \sqrt{1 - p_v} & \text{for } v = u \\ 1 - \sqrt{1 - p_{v-1}} < \alpha_{\text{cr}} < 1 - \sqrt{1 - p_v} & \text{for } u + 1 \leq v \leq S \end{cases}$

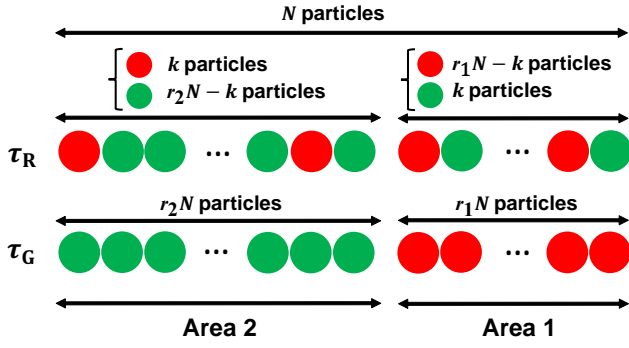


FIG. 21. (Color online) Schematic illustration of τ_G (upper panel) and τ_R (lower panel), where the red particles belong to species 1 and the green ones to species 2. In the upper panel, we show one example from among all $\binom{rN}{k} \times \binom{(1-r)N}{k}$ possible random sequences, whereas in the lower panel we show one of the two possible group sequences.

Considering that τ_R satisfying this supposition possibly has $\binom{rN}{k} \times \binom{(1-r)N}{k}$ sequences, $a_N = \sum_{\forall \tau_R} K'(\tau_G, \tau_R)$ can be written as follows;

$$\begin{aligned}
 a_N &= \sum_{\forall \tau_R} K'(\tau_G, \tau_R) \\
 &= \sum_{k=1}^{rN} k \binom{rN}{k} \binom{(1-r)N}{k} \\
 &= \sum_{k=1}^{rN} rN \binom{rN-1}{k-1} \binom{(1-r)N}{k} \\
 &= rN \sum_{k=1}^{rN} \left\{ \binom{rN}{k} \binom{(1-r)N}{k} - \binom{rN-1}{k} \binom{(1-r)N}{k} \right\}.
 \end{aligned} \tag{K1}$$

Using the Vandermonde convolution formula, Eq. (K1)

can be rewritten as follows:

$$a_N = rN \left\{ \binom{N}{rN} - \binom{N-1}{rN} \right\}. \tag{K2}$$

Because the sequence τ_R can take any of $N!/\{(rN)!((1-r)N)!\}$ possible patterns with equal probability, we can finally reduce \overline{K}' to

$$\overline{K}' = \frac{(rN)!((1-r)N)!}{N!} a_N = r(1-r)N. \tag{K3}$$

Figure 22 compares the simulation (circles) and theoretical (curves) values for various $N \in \{1,000(\text{red}), 5,000(\text{green}), 10,000(\text{blue})\}$ for $S = 2$. The simulations show very good agreement with our exact analysis.

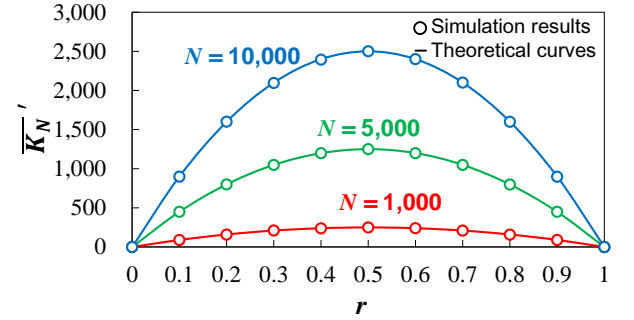


FIG. 22. (Color online) Simulation (circles) and theoretical (curve) values of \overline{K}' as functions of r for various $N \in \{1,000(\text{red}), 5,000(\text{green}), 10,000(\text{blue})\}$ with $S = 2$. We obtained each of the simulation values by averaging over 100 trials.

2. $S = N$

When $S = N$, τ_G also has to be fixed as either of the two possible patterns—an ascending or a descending sequence—for a general calculation of \overline{K}' , as illustrated in the upper panel of Fig. 23. Once τ_G is fixed,

$K'(\tau_G, \tau_R)$ can be determined uniquely for all possible τ_R .

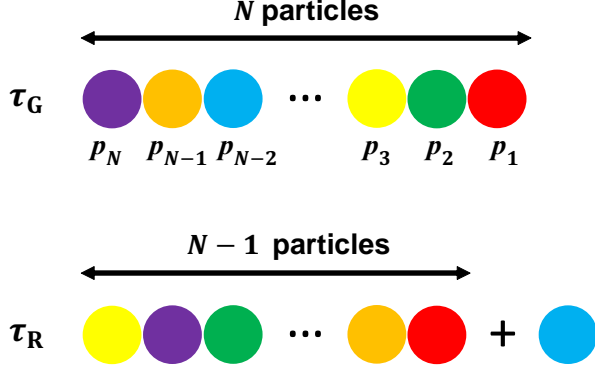


FIG. 23. (Color online) Schematic illustration of τ_G (upper panel) and τ_R (lower panel) for the case $S = N$. In the lower panel, we show one example of all $N \times (N-1)!$ possible sequences. Note that $p_1 < p_2 < \dots < p_N$ for the ascending sequence, whereas $p_1 > p_2 > \dots > p_N$ for the descending one.

If we regard the entire sequence as consisting of two parts—the first (blue) particle and other $(N-1)$ particles, as described in the lower panel of Fig. 23—the sorting procedure can also be divided into two parts: sorting $(N-1)$ particles plus the last exchange for the first particle. If the first particle corresponds to the particle with hopping probability p_l ($l = 1, 2, \dots, N$), and noting that the sequence for the remaining $(N-1)$ particles has $(N-1)!$ possible patterns, we can calculate the quantity $b_{N,l} = \sum_{\forall \tau'_{R,l}} K(\tau_G, \tau'_{R,l})$ as follows:

$$\begin{aligned} b_{N,l} &= \sum_{\forall \tau'_{R,l}} K(\tau_G, \tau'_{R,l}) \\ &= \begin{cases} a_{N-1} & \text{for } l = 1, \\ a_{N-1} + (N-1)! & \text{for } l = 2, 3, \dots, N, \end{cases} \end{aligned} \quad (\text{K4})$$

where $N > 1$ and $\tau'_{R,l}$ represents the sequence for which the first particle is the particle with hopping probability p_l . Note that the last sort is not necessary in the case where $l = 1$.

Therefore, for $N > 1$, we can write $a_N = \sum_{\forall \tau_R} K(\tau_G, \tau_R)$:

$$\begin{aligned} a_N &= \sum_{\forall \tau_R} K_N(\tau_G, \tau_R) \\ &= \sum_{l=1}^N \sum_{\forall \tau'_{R,l}} K_N(\tau_G, \tau'_{R,l}) \\ &= \sum_{l=1}^N b_{N,l} \\ &= (N-1) \times (N-1)! + Na_{N-1} \end{aligned} \quad (\text{K5})$$

Dividing both sides of Eq. (K5) by $N!$, we obtain

$$c_N = c_{N-1} + \frac{N-1}{N} = c_1 + \sum_{k=1}^N \frac{k-1}{k}, \quad (\text{K6})$$

where $c_N = a_N/N!$ and $N > 2$. With the initial condition $c_1 = a_1 = 0$, a_N is finally reduced to

$$a_N = N! \left(N - \sum_{k=1}^N \frac{1}{k} \right), \quad (\text{K7})$$

which we note holds for the case $N = 1$.

The sequence τ_R can take $N!$ patterns with equal probability, and therefore, $\overline{K'}$ is finally reduced to

$$\overline{K'} = \frac{a_N}{N!} = N - \sum_{k=1}^N \frac{1}{k}. \quad (\text{K8})$$

Figure 24 compares the simulation (circles) and theoretical (line) values for $S = N$. The simulations again show a very good agreement with our exact analysis.

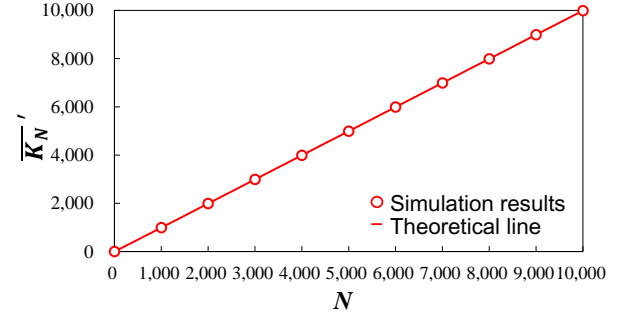


FIG. 24. (Color online) Simulation (circles) and theoretical (line) values of $\overline{K'_N}$ as functions of N . We obtained each of the simulation values by averaging over 100 trials.

-
- [1] C. Appert-Rolland, S. Klein, M. Ebbinghaus, and L. Santen, in *Proceedings of the Asia-Pacific Economics Conference 2016 Big Data Analysis and Modeling toward Super Smart Society (APEC-SSS2016)* (2017) p. 011001.
- [2] S. Croom, P. Romano, and M. Giannakis, *Eur. J. Purch. Supply Manag.* **6**, 67 (2000).
- [3] T. Ezaki, D. Yanagisawa, and K. Nishinari, *Physica A* **427**, 62 (2015).
- [4] Y. Taniguchi, R. Nishi, T. Ezaki, and K. Nishinari, *Physica A* **433**, 304 (2015).
- [5] M. Woelki, *Phys. Rev. E* **87**, 062818 (2013).
- [6] T. Imai and K. Nishinari, *Phys. Rev. E* **91**, 062818 (2015).
- [7] H. Yamamoto, D. Yanagisawa, and K. Nishinari, *J. Stat. Mech.* **2017**, 043204 (2017).
- [8] K. Christensen and Y. Sasaki, *J. Artif. Soc. Soc. Simul.* **11**, 9 (2008).
- [9] N. Pelechano and A. Malkawi, *Automat. Constr.* **17**, 377 (2008).
- [10] D. Yanagisawa, A. Kimura, A. Tomoeda, R. Nishi, Y. Suma, K. Ohtsuka, and K. Nishinari, *Phys. Rev. E* **80**, 036110 (2009).
- [11] T. Ezaki, D. Yanagisawa, K. Ohtsuka, and K. Nishinari, *Physica A* **391**, 291 (2012).
- [12] J. E. Rothman, *Nature* **372**, 55 (1994).
- [13] M. J. Müller, S. Klumpp, and R. Lipowsky, *Proc. Natl. Acad. Sci.* **105**, 4609 (2008).
- [14] P. C. Bressloff and J. M. Newby, *Rev. Mod. Phys.* **85**, 135 (2013).
- [15] C. T. MacDonald, J. H. Gibbs, and A. C. Pipkin, *Biopolymers* **6**, 1 (1968).
- [16] C. T. MacDonald and J. H. Gibbs, *Biopolymers* **7**, 707 (1969).
- [17] A. Parmeggiani, T. Franosch, and E. Frey, *Phys. Rev. Lett.* **90**, 086601 (2003).
- [18] D. Chowdhury, A. Schadschneider, and K. Nishinari, *Phys. Life Rev.* **2**, 318 (2005).
- [19] T. Chou, K. Mallick, and R. Zia, *Rep. Prog. Phys.* **74**, 116601 (2011).
- [20] C. Appert-Rolland, M. Ebbinghaus, and L. Santen, *Phys. Rep.* **593**, 1 (2015).
- [21] D. Helbing, *Rev. Mod. Phys.* **73**, 1067 (2001).
- [22] H. Ito and K. Nishinari, *Phys. Rev. E* **89**, 042813 (2014).
- [23] S. Tsuzuki, D. Yanagisawa, and K. Nishinari, *Phys. Rev. E* **97**, 042117 (2018).
- [24] D. Yanagisawa, A. Tomoeda, R. Jiang, and K. Nishinari, *JSIAM Lett.* **2**, 61 (2010).
- [25] C. Arita and D. Yanagisawa, *J. Stat. Phys.* **141**, 829 (2010).
- [26] C. Arita and A. Schadschneider, *Math. Mod. Meth.* **25**, 401 (2015).
- [27] J. de Gier and B. Nienhuis, *Phys. Rev. E* **59**, 4899 (1999).
- [28] R. A. Blythe and M. R. Evans, *J. Phys. A* **40**, R333 (2007).
- [29] B. Derrida, M. R. Evans, V. Hakim, and V. Pasquier, *J. Phys. A* **26**, 1493 (1993).
- [30] T. Minemura, K. Nishinari, and A. Schadschneider, in *International Conference on Cellular Automata* (Springer, 2010) pp. 593–599.
- [31] D. A. Adams, B. Schmittmann, and R. K. P. Zia, *J. Stat. Mech.* **2008**, P06009 (2008).
- [32] L. J. Cook, R. K. P. Zia, and B. Schmittmann, *Phys. Rev. E* **80**, 031142 (2009).
- [33] L. J. Cook and R. K. P. Zia, *J. Stat. Mech.* **2009**, P02012 (2009).
- [34] L. J. Cook and R. K. P. Zia, *J. Stat. Mech.* **2012**, P05008 (2012).
- [35] B. Aneva, *Eur. Phys. J. C* **31**, 403 (2003).
- [36] O. Angel, *J. Comb. Theory A* **113**, 625 (2006).
- [37] C. Arita, A. Kuniba, K. Sakai, and T. Sawabe, *J. Phys. A* **42**, 345002 (2009).
- [38] L. Cantini, *J. Phys. A* **41**, 095001 (2008).
- [39] B. Derrida and M. Evans, *J. Phys. A* **32**, 4833 (1999).
- [40] E. Duchi and G. Schaeffer, *J. Comb. Theory A* **110**, 1 (2005).
- [41] P. A. Ferrari, L. R. Fontes, and Y. Kohayakawa, *J. Stat. Phys.* **76**, 1153 (1994).
- [42] P. A. Ferrari, J. B. Martin, *et al.*, *Ann. Probab.* **35**, 807 (2007).
- [43] P. F. Arndt, T. Heinzel, and V. Rittenberg, *J. Phys. A* **31**, L45 (1998).
- [44] M. Evans, *Europhys. Lett.* **36**, 13 (1996).
- [45] M. Evans, *J. Phys. A* **30**, 5669 (1997).
- [46] J. Krug and P. A. Ferrari, *J. Phys. A* **29**, L465 (1996).
- [47] T. Sasamoto, *Phys. Rev. E* **61**, 4980 (2000).
- [48] K. Mallick, S. Mallick, and N. Rajewsky, *J. Phys. A* **32**, 8399 (1999).
- [49] K. Mallick, *J. Phys. A* **29**, 5375 (1996).
- [50] C. Arita, *J. Stat. Mech.* **2006**, P12008 (2006).
- [51] A. Ayyer, J. L. Lebowitz, and E. R. Speer, *J. Stat. Phys.* **135**, 1009 (2009).
- [52] V. Privman, *Nonequilibrium statistical mechanics in one dimension* (Cambridge University Press, 2005).
- [53] M. Uchiyama, *Chaos Soliton Fract.* **35**, 398 (2008).
- [54] N. Crampe, C. Finn, E. Ragoucy, and M. Vanicat, *J. Phys. A* **49**, 375201 (2016).
- [55] C. Arita and K. Mallick, *J. Phys. A* **46**, 085002 (2013).
- [56] S. Prohac, M. R. Evans, and K. Mallick, *J. Phys. A* **42**, 165004 (2009).
- [57] N. Crampe, K. Mallick, E. Ragoucy, and M. Vanicat, *J. Phys. A* **48**, 175002 (2015).
- [58] A. Ayyer and D. Roy, *Sci. Rep.* **7**, 13555 (2017).
- [59] M. Bengrine, A. Benyoussef, H. Ez-Zahraoui, J. Krug, M. Loulidi, and F. Mhirech, *J. Phys. A* **32**, 2527 (1999).
- [60] E. Duchi and G. Schaeffer, *Random Struct. Algor.* **33**, 434 (2008).